Mireia Arasa Lleixà

Ionic matrices for Mass Spectrometry Imaging of biological tissues

Treball Fi de Grau

directed by Dr. Toufik Mahamdi

directed by Dra. Maria Garcia-Altares

Degree in biomedical engineering

UNIVERSITAT ROVIRA I VIRGILI

Tarragona

2023

ABSTRACT

El análisis de metabolitos en MALDI-MSI (Espectrometría de Masas de Imagen por Desorción/Ionización Láser Asistida por Matriz) ha sido un método muy investigado, en el cual se han utilizado una gran variedad de matrices, sin embargo, se ha observado que las matrices convencionales que suelen emplearse no logran determinar adecuadamente los metabolitos de bajo peso molecular. En este proyecto se estudian las características de las matrices iónicas líquidas (ILM) para solucionar este problema. En primer lugar, se investigó la síntesis de diferentes combinaciones de ácido y base para la formación de un sólido estable, el cual será utilizado como matriz mediante la evaporación del sustrato. Esta técnica se aplicó en dos tejidos específicos, el cerebro y el páncreas de ratón. Para este estudio, se han utilizado matrices ácidas comúnmente empleadas en la MALDI-MSI, como el ácido α-cyano-4-hydroxycinnamic (HCCA) y el ácido 2,5-dihydroxybenzoic acid (DHB). Estas matrices se combinan con bases orgánicas, tales como la anilina (ANI), la N,N-Dimethylaniline (DMA) y la N,N-Diethylaniline (DEA). Finalmente mediante análisis por MALDI-MSI y con herramientas basadas en lenguaje R, se analizaron los diferentes tipos de analitos y se comparan sus intensidades respecto la matriz cristalina convencional con las ILMs en los respectivos tejidos. Los resultados reflejan que la aplicación de esta nueva matriz para detectar metabolitos de bajo peso molecular mejora la intensidad de los analitos atenuando la señal proveniente de los picos de la matriz, obteniendo así un espectro con menos ruido. Cabe destacar que, estas matrices también tienen la capacidad para detectar analitos con formación de aductos de sodio y potasio.

The analysis of metabolites by MALDI-MSI (Matrix-Assisted Laser Desorption/Ionization Mass Spectrometry Imaging) has been a well-researched method, in which a wide variety of matrices have been used, however, it has been observed that the conventional matrices that are usually used fail to adequately determine low molecular weight metabolites. This project studies the characteristics of ionic liquid matrices (ILM) to solve this problem. First, we attempted the synthesis of different combinations of acid and base for the formation of a stable solid, which was used as a matrix by thermal evaporation of the substrate. This technique was applied on two specific tissues, the brain and the pancreas from mice. For this study, acid matrices commonly used in MALDI-MSI have been used, such as α-cyano-4-hydroxycinnamic acid (HCCA) and 2,5-dihydroxybenzoic acid (DHB). These matrices are combined with organic bases, such as aniline (ANI), N,N-Dimethylaniline (DMA) and N,N-Diethylaniline (DEA), to synthesize ILMs. Finally, through analysis by MALDI-MSI and R based computational tools, the different types of analytes are identified and their intensities are compared with respect to the conventional crystal matrix with the ILMs in the respective tissues. The results show that the application of these new matrices improves the intensity of low molecular weight analytes attenuating the signal coming from the peaks of the matrix, thus obtaining a spectrum with less noise. Notably, these matrices also have the ability to detect analytes with formation of sodium and potassium adducts.

Table of abbreviations

ANI - Aniline

APC - Chemical Ionization

DEA - N,N-Diethylaniline

DESI - Desorption electrospray ionization

DHB - 2,5-dihydroxybenzoic acid

DMA - N,N-Dimethylaniline

DMAN - Naphthalene

EI - Electron Ionization

ESI - Electrospray Ionization

ESPT - Excited state proton transfer

FT-ICR - Fourier transform ion cyclotron resonance

H&E - Hematoxylin and eosin

HCCA - α-cyano-4-hydroxycinnamic acid

ILM - Ionic Liquid Matrices

IL- Ionic Liquid

IR-MALDI - MALDI using infrared lasers

K - Potassium

LA-ICP-MS - Laser ablation–inductively coupled plasma mass spectrometry

MALDI-MSI - Matrix-Assisted Laser Desorption/Ionization Mass Spectrometry Imaging

MeOH - Methanol

m/z - mass-to-charge ratio

MOB - Olfactory bulb

MPI - Multiphoton ionization

Na - Sodium

NIMS - Nanostructure-initiator mass spectrometry

Q - Quadrupole

QqQ - Triple Quadrupole

qTOF - Quadrupole-TOF

RTILs - Room temperature ionic liquid

SA - Synaptic acid

SIMS - Secondary ion mass spectrometry

TIC - Total Ion Count

TOF - Time of Flight

Table of contents

1. Introduction

In the field of biomedical research, the identification of novel biomarkers necessitates the utilization of analytical methodologies that possess both high sensitivity and enhanced throughput capabilities. As a result of that, nowadays, it is very important to develop new tools that allow us to quantify analytes with high sensibility and high accuracy. [1]

The identification of small metabolites is called metabolomics, this technique enables us to easily comprehend the profile of small molecules, thus facilitating a better understanding of tissue physiology. [2] While the field of Metabolomics research has experienced rapid progress, it presents significant research opportunities. The challenges in this field can be attributed to the nature of small molecule analyses, which differ from disciplines such as proteomics or genomics. However, unlike genes or proteins, which are studied in proteomics and possess well-established origins, small metabolites do not require high levels of amplification for detection. [3]

On the other hand, an extensive array of methods for detecting and classifying these analytes is at our disposal, each with its own set of advantages and disadvantages. The selection of a specific technique depends on the objective of our analysis. Among these techniques, which can be categorized as ionization methods and mass analyzers, are Electrospray Ionization (ESI), Electron Ionization (EI), Chemical Ionization (APC), and Matrix Assisted Laser Ionization (MALDI) as ionization methods. For mass-to-charge ratio m/z analysis, we have a range of options including Time of Flight (TOF), Quadrupole (Q), Quadrupole-TOF (qTOF), Triple Quadrupole (QqQ), Ion Trap, Orbitrap, and Fourier transform ion cyclotron resonance (FT-ICR).

In our project, we will utilize a combination of the MALDI ionization technique and the Orbitrap mass analyzer. This approach minimizes compound fragmentation through the MALDI technique while delivering high mass resolution, encompassing accuracy and an extensive mass range. It is important to note that our measurement equipment has certain limitations, including lower sensitivity and a moderate dynamic range. [3]

Furthermore, the utilization of ILMs significantly reduces the occurrence of analyte fragmentation compared to the traditional approach involving pure crystalline matrices.[3] This observation highlights the advantageous nature of ILMs in preserving the structural integrity of analytes during ionization processes, thereby minimizing the extent of fragmentation encountered in the mass spectrometry analysis.

1. 2 MALDI mass spectrometry imaging

MALDI-imaging mass spectrometry (MSI) is employed as a technique for the identification of small proteins or metabolites and their distribution in relatively complex samples.[1] [4]

MSI is a powerful analytical technique capable of elucidating valuable insights into the spatial distribution of multiple compounds within tissue samples.This approach obviates the requirement for molecular labeling or any prior staining procedures. [5] Furthermore, MSI can be seamlessly integrated with various ionization technologies, such as MALDI, MALDI using infrared lasers (IR-MALDI), desorption electrospray ionization (DESI), nano-DESI , nanostructure-initiator mass spectrometry (NIMS), secondary ion mass spectrometry (SIMS), and laser ablation–inductively coupled plasma mass spectrometry (LA-ICP-MS), enhancing its versatility and analytical capabilities. [6][7]

Significantly, the selection of the ionization method, mass spectrometer configuration, and tissue preparation protocol all exert considerable influence over the range of detectable molecules and the corresponding sensitivity of the analysis.[7]

The analysis with MALDI-MSI can determinate thousands of molecules in only one measurement and it is able to acquire the cellular profile with a very accurate precision.This method is conducive to expedited data acquisition and analysis, facilitating efficient processing of experimental results. [8] In few years, the technique has improved by doing so many practices that make it more accurate and robust. [1] This method encompasses a three-part workflow involving sample preparation, m/z spectral acquisition, and subsequent data processing.[7]

The underlying principle of MALDI-MSI is depicted in Figure X. Typically, the initial sample comprises tissue sections ranging from 10 to 20 µm in thickness, carefully positioned on a slide and coated with a matrix suitable for the targeted compound detection. The sample stage is subjected to irradiation by a fixed laser beam, resulting in the generation of a distinct mass spectrum corresponding to the specific region of the tissue that was irradiated. The molecular weight of the analytes generated by the laser is determined using a mass analyzer, in our case using Orbitrap.[10] This technique enables the acquisition of numerous mass spectra from a given tissue section. [6] [8]

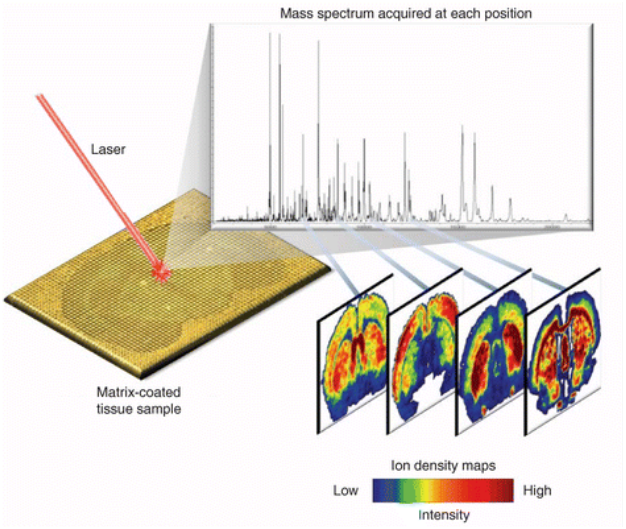

Figure 1: MALDI-MSI principe workflow **[9]**

The orbitrap is a mass analyzer, initially discovered in 1923 by Kigdon, consists of a triad of electrodes. These electrodes are spatially separated by a nanometer-scale gap containing a dielectric material, ensuring electrical isolation. By applying a voltage across the external electrodes and the central electrode, a linear electric field is generated, promoting the formation of stable oscillations along the axis. Simultaneously, the radial component of the electric field induces the attraction of ions towards the central electrode.[11] (Figure 2)

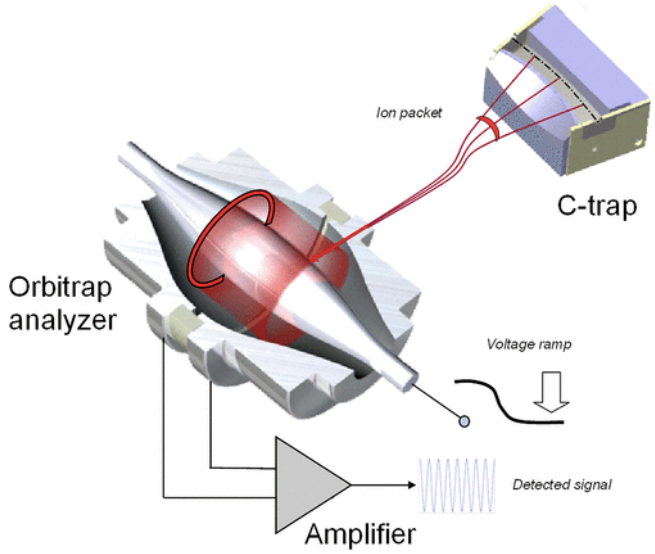

Figure 2: Orbitrap principe. The ions are stored in the doubled quadrupole (C-trap), and then a high voltage is applied to detect the m/z of the analytes and classify them into packets. The C-trap packets are directed to the analyzer during the voltage ramp, where they propagate through the oscillating rings, inducing a current that is detected by the differential amplifier. [13]

1.3 Matrix in MALDI-MSI

For proper analysis by MALDI-MSI, it is crucial to consider the proper collection and treatment of the sample. This implies the careful application of a matrix, ensuring its uniform distribution throughout the sample. A wrong application of the matrix can lead us to wrong results.[6] The matrix applied to the sample is tailored specifically based on the analytes targeted in our study. [8]

Synaptic acid (SA) demonstrates utility in detecting high molecular weight proteins, while α-cyano-4-hydroxycinnamic acid (HCCA) is commonly employed for the detection of low molecular weight proteins or peptides. Conversely, 2,5-dihydroxybenzoic acid (DHB) offers the advantage of facilitating the detection of oligosaccharides and nucleotides, contrary to HCCA. [8][12]

Once the sample has already been homogeneously covered by the matrix, co-crystallization takes place. The resulting crystals, in conjunction with laser energy, significantly influence the image resolution and subsequent analysis outcomes. Therefore, it is crucial to underscore the criticality of selecting an appropriate matrix based on the specific measurement objectives and its properties.

Matrices composed of inorganic nanoparticles have been developed for the analysis of specific small molecules. Matrices such as colloidal silver 35 and colloidal graphite 36 have been used in the detection of lipids. In particular, certain matrices, such as ILM, offer significant advantages. One such matrix is the powerful 1,8-bis(dimethylamino)naphthalene (DMAN) base, which effectively reduces the peak intensity of the matrix, resulting in decreased noise levels during measurement of the analyte. Another matrix of interest for MALDI-MSI applications is SA. [8]

Furthermore, comprehensive mapping of analyzes across the entire sample can be achieved by analyzing the m/z distribution throughout the tissue ,this characteristic can be highly useful for diagnostics or prognostics.[13]

Table 1: matrix's requirements to be suitable for MALDI analysis [19]

1	Should have high absorption at the same waveleght of the laser radiation
2	Capability to protonate or deprotonate the target analyte
3	Effectively ionize the target analyte
4	Effectively ionize all analytes in a mixture without or with minimal ion suppression.
5	No fragmentation of the analytes
6	Avoid the formation of adduct species with the investigated analytes.
7	Must be miscible with the analyte solution and co-crystalize with the investigated analytes.
9	Have high reproducibility with very low relative standard deviation (RSD) from spot to spot.
10	Avoid any change in the analytes's chemical structure
11	Cheap and avoid toxicity

The use of MALDI as ionization requires the use of a matrix to promote the desoption/ionization of analytes. In this case the ILMs are matrices composed of an acid and a base that form a salt. They have been employed in MALDI-MSI as a matrix for the detection and quantification of low molecular weight metabolites, as well as other molecules such as peptides and oligodeoxynucleotides. [14][15]

1.4 Matrix application methods

Regarding the application of the matrix, various techniques have been developed to enhance the dispersion of analytes resulting from matrix deposition. Among these methods are sublimation and deposition, which are employed to facilitate the matrix application process. [8]

One of the matrix application technique that provides homogeneous deposition is achieved by using a deactivated glass spray nebulizer, where the matrix is sprayed directly onto the sample. The aim of this procedure is to improve matrix co-crystallization with the tissue and minimize analyte delocalization from the tissue. The procedure involves multiple cycles of spraying the matrix onto the sample, which is placed on a platform at a distance of approximately 20-30 cm. The platform is carefully moved to ensure uniform distribution across the entire sample. Afterwards, the sample is allowed to dry for 1 - 2 minutes , and as mentioned before, this process is repeated approximately ten times to ensure proper matrix deposition. The cycles of this procedure are designed to prevent sample drying and preserving its properties throughout the process. [13]. These techniques enable us to acquire the m/z spectrum of each analyte by employing laser ablation techniques, or the spectrum of multiple analytes at that point.

It is however desirable to apply the matrix coating by dry techniques, i.e. without the presence of solvents that could cause delocalization of analytes on the tissue. For instance, thermal evaporation (Figure 3) is a dry technique that consists of depositing a thin layer onto the sample by evaporating a solid compound at high temperatures. This process promotes the volatilization of matrix particles, which subsequently reach the upper surface where the sample is located. Upon contact with the sample, these vaporized particles undergo a phase change, forming a solid layer. The technique employs a resistive coil to achieve the necessary melting points. By exposing the coil to a continuous current and with certain vacuum conditions, the desired melting points can be reached in shorter time periods, facilitating the deposition of the substrate onto the sample.[16]

Two types of sources can be used, a refractory wire or a crucible, which are electrically heated and contain the material to be evaporated, in this case, the matrix. This method requires a high-vacuum chamber with pressures below 10-2 Pa to prevent oxidation of the source. Additionally, this process is conducted under these conditions to ensure rapid evaporation without damaging the source or crucible. The properties of the particles of the deposited material may be different depending on the method used to heat them.[23]

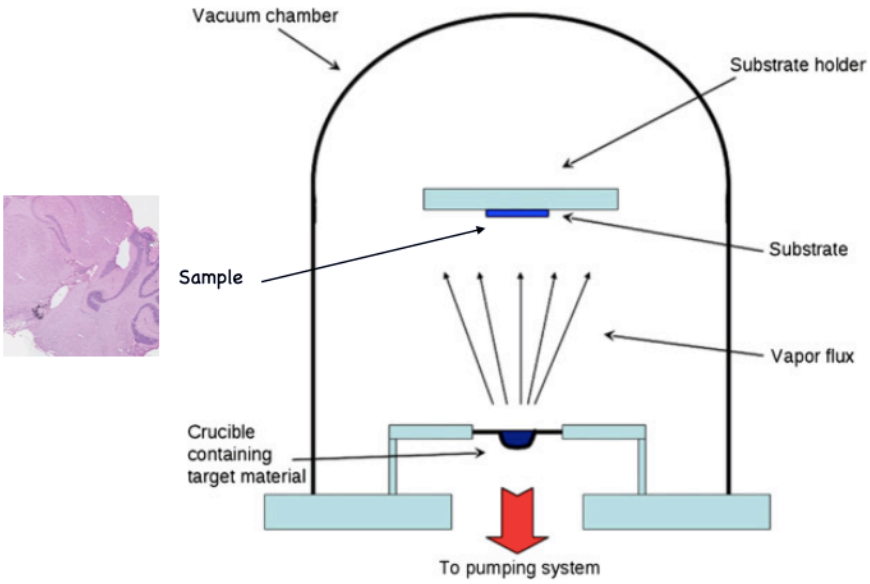

Figure 3: Diagram of the evaporation procedure of the matrix by means of thermal evaporation [21]

1.5 Ionic Liquid matrices

Conventional matrices exhibit certain disadvantages, including the generation of numerous low-intensity peaks originating from matrix protonation/deprotonation during the evaporation phase, fragmentation, and group formation. In addressing this issue, ILMs present a potential solution. ILMs comprise a combination of diverse conventional matrices and offer notable benefits such as enhanced crystallization homogeneity, improved spectral resolution, higher signal intensity compared to conventional matrices, and increased reproducibility. [8]

Ionic liquids (IL) possess highly favorable physicochemical characteristics for their application as matrices in MALDI imaging. Among these properties we can find low melting points, as they melt at temperatures below 100ºC, exceptional thermal stability, wide temperature tolerance, as they are stable at temperatures below 250ºC, they are not explosive or flammable and have negligible vapor pressures.[17][18]

These properties have the ability to be adjusted based on research goals, which can be achieved by altering the cations or ions present in the IL. By way of illustration, nitrate serves as an anion used as a counterions to manipulate the aforementioned properties. This gives unlimited opportunities to manufacture custom matrices that encompass various characteristics, including drying properties, melting points, polarities, or viscosity.

In a study conducted by Zabet-Moghaddam et al. [18], it was demonstrated that due to the inherent characteristics of ionic liquid, in combination with conventional MALDI matrix compounds, they became a potential matrix for the analysis of analytes using MALDI-MSI.[18]

On the other hand, Armstrong et al. [18] ,as a result of the investigations of ILs, introduced a novel class of matrices termed Class II ionic liquids. These matrices consist of organic salts which are formed by equimolar combination of conventional MALDI matrices, also referred to as crystalline matrices. Showcases of such matrices encompass HCCA, CCA, DHB, or SA, serving as acidic components in conjunction with organic bases like tributylamine, aniline, or pyridine. Class II ionic liquids can be categorized into two distinct classes: room temperature ionic liquids (RTILs) and ILMs. In contrast to RTILs, ILMs exhibit superior suitability for employment as MALDI matrices. [18][19]

There are mainly two ways to synthesize organic salts. The first and commonly used method is the combination of a methanolic solution with an acidic component and an organic base, followed by the application of sonic energy to agitate the sample particles and finally complete solvent removal. Subsequent boiling of the sample has shown benefits in terms of conversion to ILM, such as improved stability. This salt can be redissolved and used for sample preparation. As for the second method, it has some disadvantages as it may not provide an equimolar solution, leading to an imbalance between the two components of the matrix. This can result in potential system contamination under vacuum or poor crystallization.[18][20]

ILMs possess a highly advantageous characteristic when it comes to matrix deposition on the sample, as they allow for achieving a significantly favorable homogeneity. Partially crystallized matrices exhibit greater homogeneity compared to conventional solid matrices. Furthermore, in conventional matrices, it is challenging to detect analyte signals in different tissue regions, whereas this effect is reduced with ILMs. It was also observed that samples treated with ILMs had the ability to withstand a higher number of laser shots at a specific position. This can be particularly useful when conducting measurements that require a larger number of shots than the typically established limit. [18]

1.6 MALDI imaging for small molecule identification or metabolomics

One of the disadvantages of conventional ion matrices during analysis is the interference they cause in the lower m/z range (<1000 Da) due to auto-ionization. In addition, they also generate interference from peaks in the matrix, leading to overlapping peaks and increased noise in the analysis.

In this work, we demonstrate that the use of ILM for MALDI-MSI analysis is highly beneficial for the determination of low molecular weight molecules. ILMs reduce or even eliminate interference peaks that arise when running samples with conventional matrices. However, it is crucial to carefully select the acid-base conjugate used for matrix synthesis, as a good choice can provide high intensity for target analytes and significant reduction in interferences. Furthermore, these matrices, by not exhibiting adducts signals, provide a more accurate calculation of the molecular weight. [18][20]

The ion deformation mechanism depends on different parameters such as; the properties of the laser, the wavelength at which the matrix absorbs, the energy of the photon, the irradiance of the laser, the angle of incidence, the exposure time of the sample to the laser, the type of matrix that we use, the printers and sample preparation methods. [20]

Due to the recent utilization of ILMs for this purpose, when talking about the ionization mechanism that concerns them, it is not well defined. However, multiple ionization mechanisms have been described.

These mechanisms, along with other techniques, form the basis of MALDI-MSI analysis.The first technique is the formation of primary ions, such as multiphoton ionization (MPI) or excited state proton transfer (ESPT). The second technique presented is secondary ion formation, which induces H+ proton transfer, electron capture, cationization, electron transfer, and ejection. A third method introduced is the "Lucky Survivor", which postulates that ionization takes place in solution and that the spices retain their charge in that state and exist as predominant ions within the matrix. Finally, the fourth technique is specific to UV-MALDI and does not involve contributions from electronic excitation in ionization. [20]

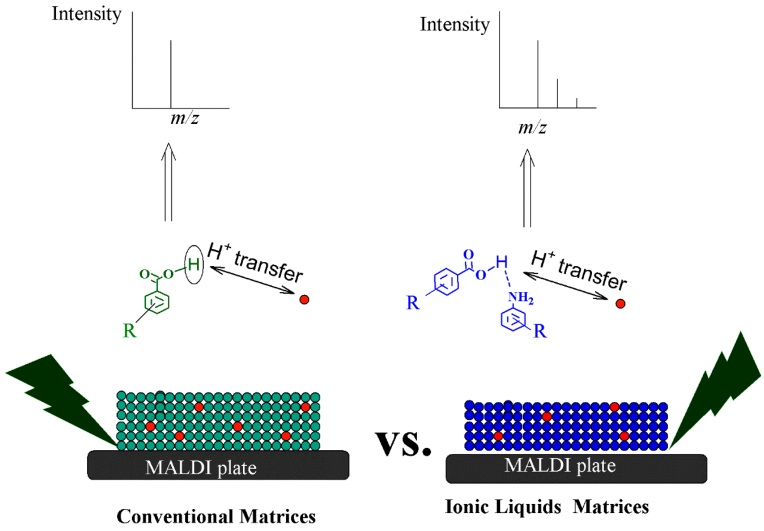

Figure 4: Proton ionization on a conventional matrix compound (such as DHB) versus an ionic liquid matrix and the final spectra (m/z / intensity) [20]

These mechanisms were described for the use of conventional organic matrices, although they may also be applicable for the use of ILM. (Figure 4)

Among the different analysis methods there are different sources of desorption/ionization, MALDI offers us a sensitivity and spatial resolution but it depends directly on the selection or application of the matrix. Compared to the other methods, such as SIMS and DESI, MALDI avoids the fragmentation of the analytes which makes it easier to identify them. [22]

To accomplish accurate quantification using MALDI, it is necessary to have controlled and stable Total Ion Count (TIC), as well as a calibration curve that relates ion intensities to analyte concentrations, while keeping matrix peaks values below critical levels. Unlike conventional crystalline matrices, when utilizing ILM in MALDI-MSI, they exhibited a stable and controlled TIC, enabling the detection of low molecular weight analytes, peptides, proteins, oligonucleotides, and phospholipids. Moreover improves the detection of the analytes in the sample, its sensitivity, offers us greater selectivity and reduces the intensity of ions caused by unwanted factors.[20]

One of the most important characteristics we have discussed about ILMs is their homogeneity, which results in an improved analysis of signal intensities. This leads us to conclude that the combination of these two sample processing and analysis methods is highly favorable for accurate results. Zabet-Moghaddam and colleagues [20] demonstrated that by integrating these methods, a reduction in time can be achieved. Besides, measurements can be performed using fixed laser energies, which is highly beneficial for the detection of low molecular weight compounds that provide important biological information, such as amino acids, sugars, or vitamins.[20]

2. Aim of this work

The main aim of this project is to investigate the advantages of ionic liquid matrices (ILM) for MALDI imaging of metabolites.

In order to accomplish that, the first goal was is to synthesize the ILMs based on two common used matrices for MALDI; α-Cyano-4-hydroxycinnamic acid (HCCA) and 2,5-Dihydroxybenzoic acid (2,5-DHB). We investigated the suitability of the produced ILMs for dry deposition using a thermal evaporator and further MALDI image analysis.

The second goal was to successfully perform the MALDI imaging analysis. This aspect was accomplished through examination the performance of ILMs to obtain MALDI images of metabolites in murine pancreatic and brain tissues, in comparison with conventional matrices.

3. Materials and Methods

3.1 Materials

α-cyano-4-hydroxycinnamic (HCCA), 2,5-dihydroxybenzoic acid (DHB), N,N-Dimethylaniline (DMA), N,N-Diethylaniline (DEA),Aniline (ANI)and Methanol (MeOH) were purchased from Sigma-Aldrich. Microscope slides were purchased from Epredia and Conductive ITO-coated slides were purchased from Bruker.

3.2 Tissue Sampling

Bovine liver bought at the butcher shop was saved in the freezer at -80 ºC then was transferred into a +4 ºC fridge. First the liver was cut and put in micro-tubes containing three metal beads. Homogenization of the liver tissue was prepared by using the homogenizer FastPrep-24 (provider: M.P Biomedicals, Irvine California, USA) where we set the speed at 4 rpm for 15 seconds. Finally the metal beads were removed and the micro-tubs were submerged in cold water and then transferred to the freezer at -80 ºC.

The pancreas tissue used in the study were obtained from collaborators of the Pere Virgili Health Institute as leftover tissue from other experiments that passed their ethical committee. They were stored in the freezer at -80 ºC until the analysis.

The brain tissue used in this study were obtained from C57BL/6 mice from collaborators of CIBER-DEM as leftover tissue from other experiments that passed their ethical committee, flash-frozen on dry ice and stored in the freezer at -80 ºC until the analysis.

All tissue samples were sectioned at -20 ºC using a CryoStar NX50 cryostat at 10 µm thickness. Then the tissue sections were mounted onto indium tin oxide (ITO-coated) and microscope slides and stored in the freezer at -80 ºC.

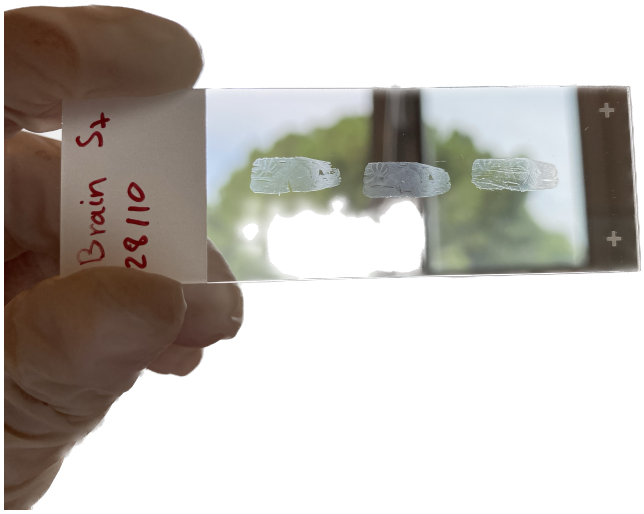

Figure 5. 10 µm layer of brain tissue.

3.3 Synthesis of Ionic Liquid Matrix

Matrix solutions were prepared by dissolving 1000 mg of HCCA or DHB in 50 ml of methanol and then vortexed for 5 minutes. Six ILM solutions were prepared for each matrix following the same procedure. One equimolar of organic base (ANI, DMA, DEA) was added to the matrix solution(HCCA or DHB) to form 1:1 (acid/base) equimolar solution. The solution was then vortexed for 20 minutes. Further the solvent (MeOH) was evaporated under nitrogen stream.

Figure 6. Process with which we obtain the matrix in solid form, evaporating the solvent with liquid nitrogen.

3.4 Matrix deposition by thermal evaporation

For the matrix deposition with nanoPVD evaporator by Moorfield, 2/3 of the crucible was filled up with the matrix powder and then placed into the LTE source. When the chamber was pumped, we heated up the source to 55 ºC and opened the source shutter. Then, we increased the temperature by five until it reached the evaporation point of the matrix (Table 2). Further, we opened the substrate shutter and set substrate rotation at 2, to get an evenly distributed layer. Next the software ,where we calculate the thickness based on the sensor we have inside the chamber, has to be clean (name of the software?). Once the desired thickness was achieved, the source and substrate shutters were closed. Subsequently, the temperature was set to 0 ºC, and the chamber was vented. It should be noted that the chamber can only be vented when the temperature is below

100 ºC.

Table 2 : Evaporator parameters for each matrix.

Matrix	Temperature	Thickness
HCCA	100 ºC	10.000 ºA
DHB	80 ºC	15.000 ºA
HCCA+DMA	118 ºC	10.000 ºA
HCCA+DEA	112 ºC	10.000 ºA
DHB+ANI	100 ºC	15.000 ºA

3.5 MALDI imaging analysis

A dual-ion funnel MALDI/ESI injector (Spectroglyph, Kennewick, WA) equipped with Orbitrap Exploris 120 (Thermo Fisher Scientific) was used for MALDI imaging analysis.
Laser intensity was 1,70 Ampere was used for all the tissue covered with HCCA base matrix, and 1,75 for all the tissue covered with DHB base matrix. The spectra were acquired in the m/z range 50 to 700 Da for MALDI imaging of all the cases. All analyses were performed at 30 µm spatial resolution and 60.000 mass resolution in positive ionization mode for all of the ILMs. MSI datasets processing, and MSI image reconstruction and visualization were performed with the rMSI2 R package (https://github.com/prafols/rMSI2).

In order to identify analytes with accuracy and precision, we generated multiple databases (found in the annex of this work) encompassing diverse low molecular weight compounds. These databases were established to facilitate comparative analysis of our experimental data, allowing for the detection of analytes that exhibit matching mass values within a tolerance of 5 parts per million (ppm). By employing this approach, we aim to enhance the reliability and specificity of our analyte identification process, as the stringent mass error threshold minimizes the likelihood of false positive identifications.

We have specifically created three distinct databases, each comprising various columns. These columns include the theoretical m/z (mass-to-charge ratio), the chemical formula, the compound name, and the ion adduct classification. Within the ion adduct classification, there are four distinct classes: the protonated ion [M+H], the sodium ion adduct [M+Na], the potassium ion adduct [M+K], and the dehydrated ion adduct [M-H2O+H].

4. Results and discussion

4.1 Ionic liquid matrices: synthesis and evaluation of their aggregation

We synthesized six ILMs solutions, by adding an equimolar base (DEA, DMA, and ANI) to the matrix solution (HCCA and DHB). We further performed different solvent evaporation methods, where the evaporation by nitrogen gas stream produced the best results (data not shown). However, solvent (ethanol) evaporation step led to different final material states, where some ILMs were in liquid and three were solid, including the ILMs HCCA-DEA, HCCA-DMA, and DHB-ANI (Table 3). Since we used thermal evaporation as a matrix deposition method, we pursued our investigation with only solid ILMs (HCCA-DEA, HCCA-DMA, and DHB-ANI).

Then, we aimed to experimentally optimize the evaporation procedure for each ILM using the thermal evaporator. The experimental selection of the evaporation temperature for the utilized ILMs was facilitated by a quartz sensor, employed to measure the thickness of the deposited materials. Gradual increments of 5°C in the source temperature were implemented until reaching a point where the deposition rate monitored by the quarz sensor exhibited an increase and subsequently stabilized. This temperature was identified as the evaporation temperature specific to the respective ILM. In terms of thickness, we opted for the same thickness as that employed with conventional organic matrices that was determined as 10.000 A and 15.000 A for HCCA and DHB respectively in previous studies in the research group.

Table 3: Describe the difference matrices we try to synthesis and if that work.

Matrix	State of aggregation
HCCA+DMA	SOLID
HCCA+DEA	SOLID
HCCA+ANI	LIQUID
DHB+DMA	LIQUID
DHB+DEA	LIQUID
DHB+ANI	SOLID

4.2 MALDI-MSI of small molecular weight compounds

4.2.1 Analysis of the peaks related to the ionization of the matrix

In order to investigate the advantages of the ILMs over the conventional matrices, we performed (MALDI-MSI) analysis of mouse brain and pancreas tissue coated with organic matrices and ILMs, using thermal evaporation. The first factor that we studied to compare the two samples (HCCA and HCCA-DEA) was the matrix related ions production, which are due to the interference created by the matrix when the matrix compounds themselves get ionized.

Figure 7 represents MALDI-MSI comparison data of the signal intensity of HCCA matrix adducts; the ion m/z 172.0394 [HCCA-H2O+H]+ (Fig. 7a) it is virtually undetectable with ILMs, the ion m/Z 190.04 [HCCA+H] (Fig. 7b) is practically imperceptible with the ILMs, the ion m/z 211.0245 [HCCA+Na] (Fig. 7c) gives a slight signal but much lower than that of the conventional matrix and the ion 226.9985 [HCCA+K] (Fig. 7d) when employing the ILMs, the ion yields a minute signal, indicating its extremely low detection sensitivity.

The results show that the signal intensities of the HCCA matrix adducts ([M-H2O+H]+, [M+H]+, [M+Na]+, AND [M+K]+) significantly decreased when tissue is covered with HCCA-DEA matrix compared to HCCA matrix.

Figure 8 represents MALDI-MSI comparison data of the signal intensity of DHB matrix adducts; the ion m/z 137.0239 [DHB-H2O+H]+ (Fig. 8a) exhibits an approximate 60% reduction in signal intensity compared to the conventional measurement methodology, the ion m/z 155.0345 [DHB+H] (Fig. 8b) decreases in intensity significantly when we use ILM, the ion m/z 191.9825 [DHB+K] (Fig. 8c) it gives us a signal higher than the other ions but lower than that of the conventional matrix and the ion 226.9985 [2DHB-2H2O+H] (Fig. 8d) provides a diminished signal; however, there is no substantial disparity observed when compared to the conventional method.

The results show that the signal intensities of the DHB matrix adducts ([M-H2O+H]+, [M+H]+, [M+Na]+, AND [M+K]+) in almost all the cases decreased when tissue is covered with DHB-ANI matrix compared to DHB matrix.

Thus, we observed that adding the base DEA and ANI to the conventional matrix HCCA and DHB, respectively can decrease the signal intensity or even full suppression of the matrix related peaks.

This represents a substantial advantage over the previous technique as the utilization of the ILMs minimizes the interference of matrix ions with the analyte signal, thereby facilitating mass spectrum interpretation. This reduction in matrix interference ensures a higher signal-to-noise ratio and enables the identification and analysis of analytes with greater precision and sensitivity. Consequently, this advancement in methodology significantly enhances the robustness and reliability of the analytical process, rendering it a valuable tool in various scientific applications.

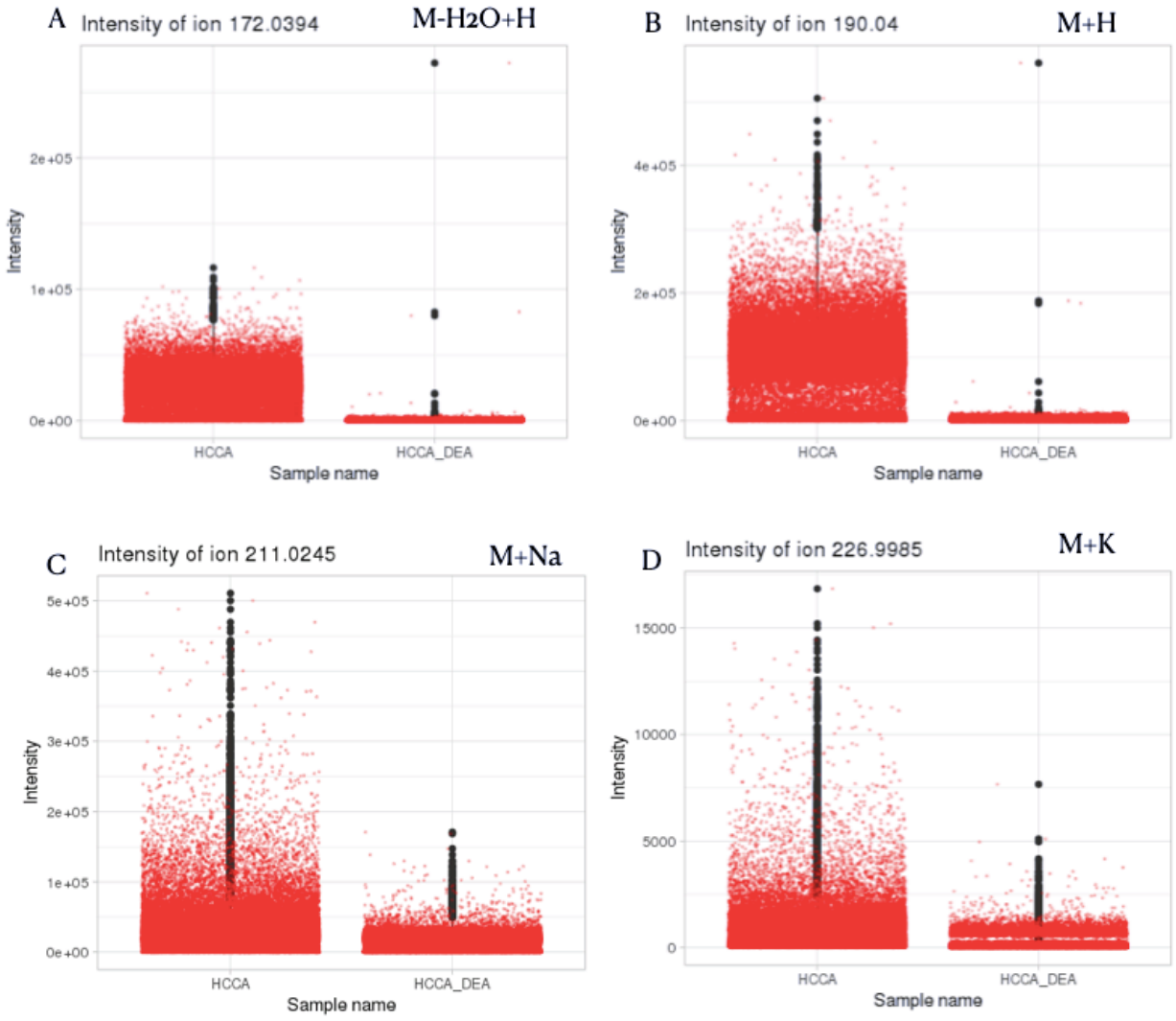

Figure 7: Boxplots representing the intensity of matrix ion signals detected on mouse brain tissue coated with 10,000 A thickness of HCCA and HCCA-DEA, measured in positive mode; a) intensity of ion m/z 172.0394 ([HCCA-H2O+H]+); b) intensity of ion m/z 190.04 ([HCCA+H]+); c) intensity of ion m/z 211.0245 ([HCCA+Na]+); d)intensity of ion m/z 226.9985 ([HCCA+K]+).

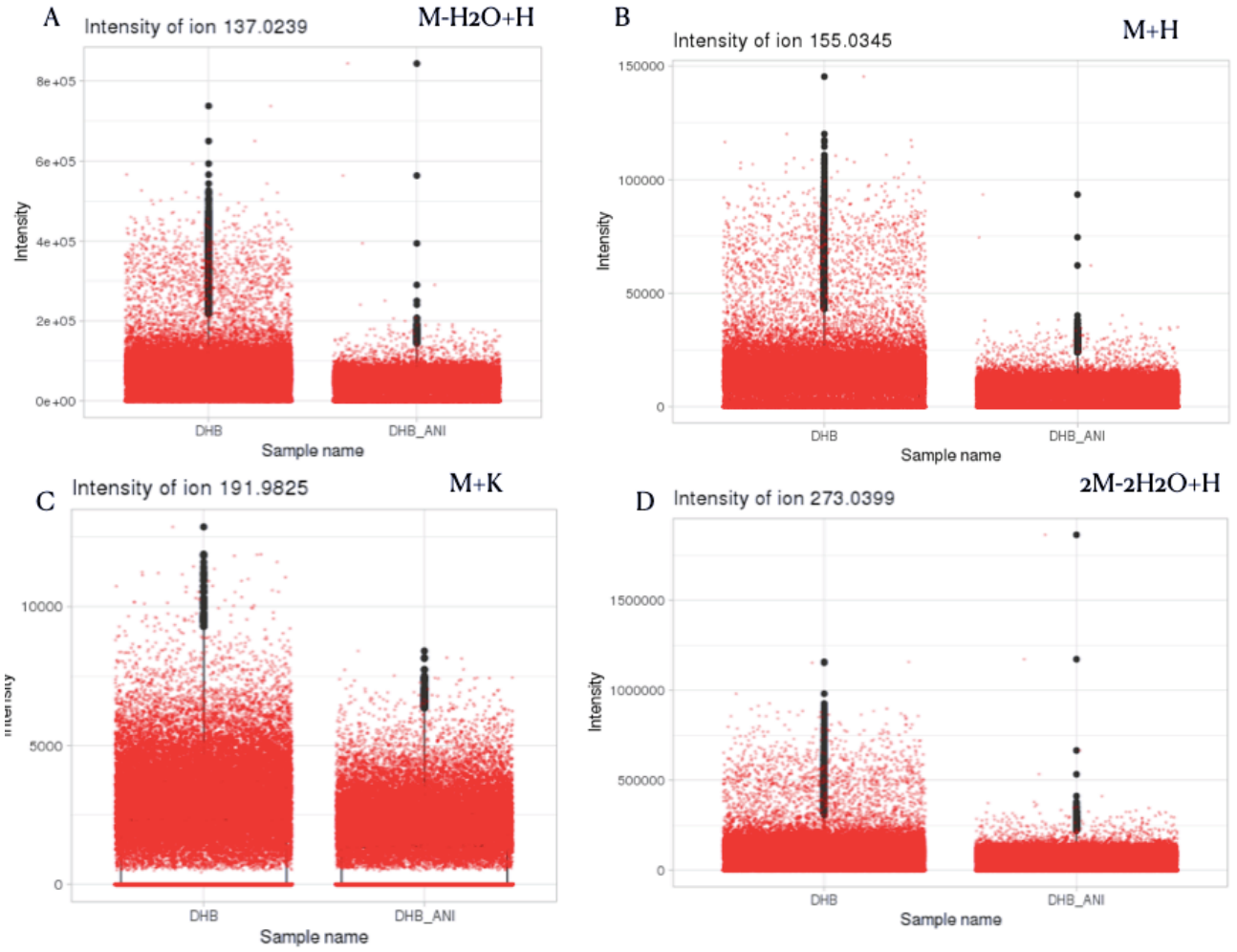

Figure 8: Boxplots representing the intensity of matrix ion signals detected on pancreas tissue coated with 10,000 A thickness of DHB and DHB-ANI, measured in positive mode; a) intensity of ion m/z 137.0239 ([DHB-H2O+H]+); b) intensity of ion m/z 155.03445 ([DHB+H]+); c) intensity of ion m/z 191.9825 ([DHB+Na]+); d)intensity of ion m/z 273.0399 ([2DHB+2H2O+H]+)**.**

4.2.2 MALDI-MSI of brain using HCCA and HCCA-DEA as matrices

4.2.2.1 Analyze of the signal intensity

The concept of Total Ion Count (TIC) refers to the cumulative intensity measurement obtained from the detection of ions across all points within a given sample. In other words, it represents the average intensity value calculated by summing up the intensities recorded at each individual point on the sample surface. This provides a holistic representation of the overall ion abundance present within the sample, offering valuable insights into the composition and distribution of ions across the analyzed area. By considering the TIC, researchers can gain a comprehensive understanding of the ionization characteristics and overall ion content within a particular sample, aiding in the interpretation and analysis of the data obtained from techniques such as mass spectrometry (Figure 9A). When comparing the conventional matrix (HCCA) with the ILM (HCCA+DHB) for brain tissue, it was possible to observe that the conventional matrix shows us a better intensity, this is due to the fact that the ILM decreases the intensity peaks of the matrix at a difference from the conventional matrix.

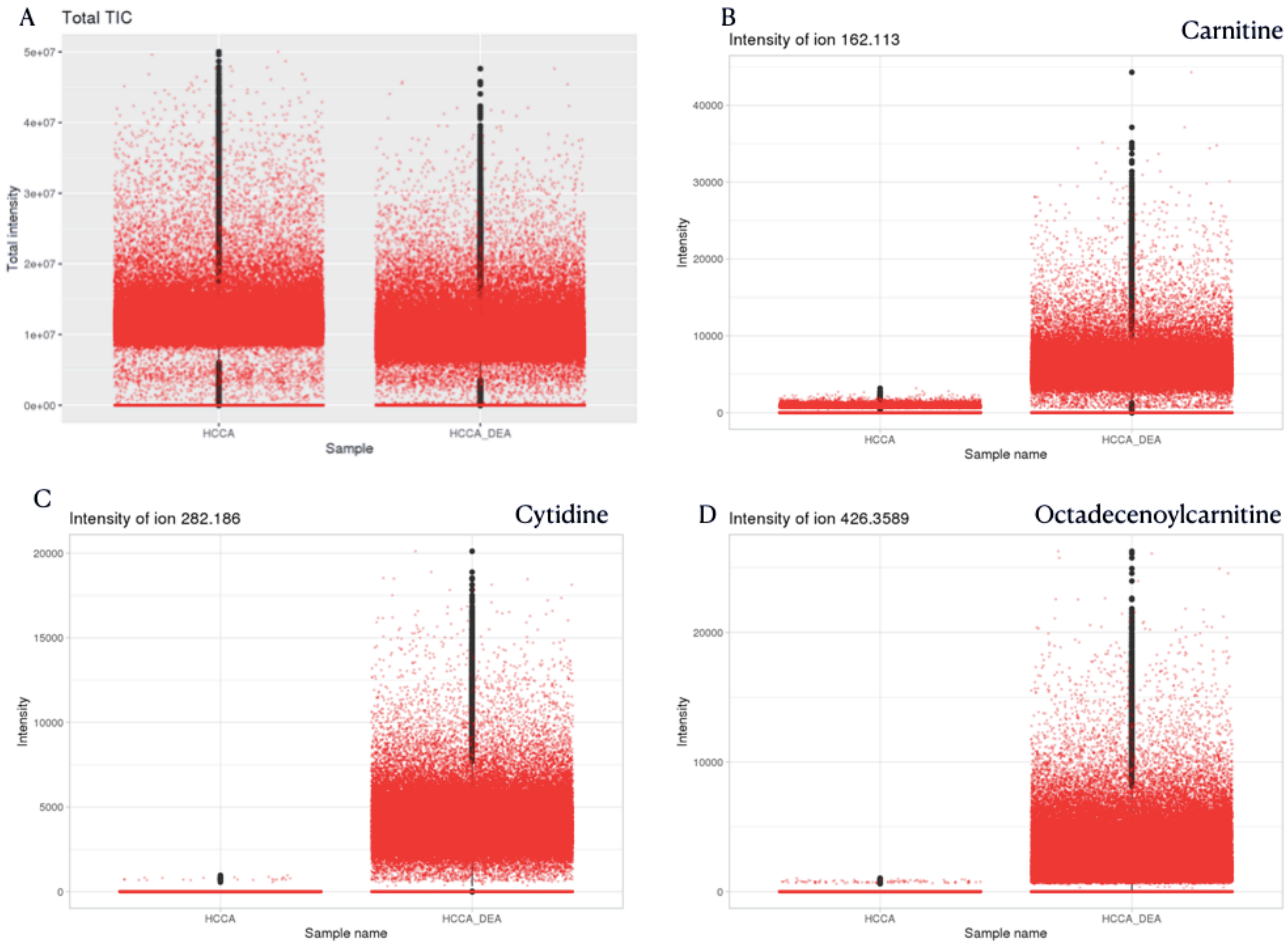

Figure 9: Boxplots representing the intensity of tissue analytes signals detected on brain tissue coated with 10,000 A thickness of HCCA and HCCA-DEA, measured in positive mode; a) total ion count ; b) intensity of ion m/z 162.113 (Carnitine); c) intensity of ion m/z 282.186 (Cytidine); d)intensity of ion m/z 426.3589 (Octadecenoylcarnitine)**.**

Figure 9 illustrates a MALDI-MSI comparison depicting the intensity of analyte signals within brain tissue coated with a uniform thickness of 10,000 Å for both ILMs and DHB matrix; (Fig. 9a) the TIC plot reveals that the HCCA matrix exhibits higher intensity compared to the HCCA+DEA matrix. This discrepancy can be attributed to the fact that the TIC plot takes into consideration all signals originating from both the matrix and the analytes. Additionally, previous experiments have indicated that the incorporation of ILMs leads to a reduction in the intensity of the matrix peaks; the analyte m/z 162.113 (Carnitine) (Fig. 9b) with the HCCA matrix, the analyte exhibits an almost negligible detection signal. Whereas it demonstrates a pronounced intensity when utilizing the alternative matrix; the analyte m/z 282.186 (Cystidine) displays near-undetectable signal levels when employing the conventional method. In contrast, it exhibits a substantial increase in intensity when utilizing the ILMs and the analyte m/z 426.3589 (Octadecenoylcarnitine)demonstrates a remarkably elevated intensity when subjected to the ILM, while exhibiting near-undetectable levels when utilizing the conventional matrix

Based on the observations depicted in Figure 9, a notable increase in the intensity of the analyte peaks is evident with the HCCA+DEA matrix compared to the conventional HCCA matrix. Furthermore, the classic method failed to detect low-weight molecules such as Cytidine (Fig 9c) and Octadecenoylcarnitine (Figure 9d). In contrast, the implementation of Ionic liquid matrices (ILMs) enabled the successful detection of these low-weight molecules with significantly higher intensities.

4.2.2.2 Metabolite identification

MALDI-MSI analysis of ILM-coated brain section (HCCA-DEA) improved analyte ionization and led to higher metabolite detection compared to conventional matrix (HCCA-DEA), a significantly higher number of analytes, specifically twenty-five, were successfully detected with the HCCA-DEA matrix compared to the previous method, which yielded the detection of only sixteen analytes (Table 4).

The majority of the detected analytes using both the ILMs and the conventional technique were identified as protonated molecules. However, it is noteworthy that the detection of cation-potassium ion adduct and the cation-sodium ion adduct was specific to the ILM approach, whereas such detection was not achieved using the conventional matrix.

Table 4: Analytes were classified into different classes base on the formation of ion adducts with brain tissue

HCCA-DEA		
Ions aducts	**Analytes detected with ILM**	**Analytes detected with HCCA**
M+H	12	11
M+Na	9	1
M+K	3	0
M-H_20+H	1	4
Total detected	25	16

Within the 4 table, we observe the targeted ion adducts investigated in our project. These ionic adducts encompass various species, including M+H (cationic adduct with a hydrogen ion), M+Na (cationic adduct with a sodium ion), M+K (cationic adduct with a potassium ion), and M-H2O+H (anionic adduct formed through water loss and hydrogen ion addition). In conjunction with these adducts, we implement a differentiation strategy that revolves around identifying specific ions, particularly those associated with amino acids. This information is meticulously outlined in the annex () with comprehensive details.

This table presents the analytes detected in brain tissue using HCCA-DEA matrix, in comparison to the use of HCCA as the matrix. In terms of the detection of protonated analytes, both matrices yielded comparable results, with minimal variations observed specifically with the ILM matrix. In the case of M+Na adducts, we observed a remarkable enhancement in detection sensitivity when employing the ILM. The M+K adducts exhibit incomplete detection when using the HCCA matrix, while conversely, the M-H2O+H adducts demonstrate higher detection sensitivity with HCCA compared to the ILM.

When comparing the extended tables present in the annexes, it can be seen that the use of ILMs gives us the ability to detect a greater number of lipids compared to the use of the conventional matrix. In addition, with ILM, we can also detect analytes of the acylcarnitine family. Another interesting finding is that ILM allows us to identify the analyte taurodeoxycholic acid with a mass of m/z of 538.3957, which belongs to the bile acid family. As for peptides, although the difference is less noticeable, with ILM we can find more varieties.

On the other hand, when analyzing brain tissue, it was found that using the conventional matrix a neurotransmitter called 5-Hydroxyindoleacetic acid with a mass of m/z of 192.0653 can be detected. However, with the use of ILM no neurotransmitter could be found in this specific case.

4.2.2.3 Image quality

Figure 10 demonstrates the distinct differentiation of various brain regions with ease. The analyte m/z 129.1386 (glutamine) (Fig 10a) is evident that exhibits a significant intensity and a well-defined structural profile; in the image of the analyte m/z 307.1800 the cerebellar region is more prominently discernible, while the frontal part of the brain, the olfactory bulb (MOB) exhibits enhanced definition compared to the analyte observed in the previous image; the analyte m/z 432.3043 tri peptide (FNL) (Fig. 10c) shows that the utilization of the ILM results in a more pronounced definition of the structural features of the analytes when compared to the conventional matrix, that in some cases is not even able to ionize/desiopt the analyte.(Figure 10)

Figure 11 illustrates a comparative analysis between a previously observed analyte, specifically m/z 129.1386 (glutamine) (Fig 11a), and its detection utilizing the conventional matrix. Additionally, in Figure 11b, we observe the presence of m/z 296.1846 (Heptanoylcarnitine), which remains undetectable when utilizing the conventional matrix.

By comparing the image obtained with the analyte m/z 129.1386 (glutamine) (Fig 10a) with a microscopy image obtained through histological staining (H&E staining) (Fig. 10d), and juxtaposing the obtained information with an image representing the anatomical references of the brain (Fig 12), we aim to discern and interpret the observable structures of the brain. In doing so, the following observations can be made.

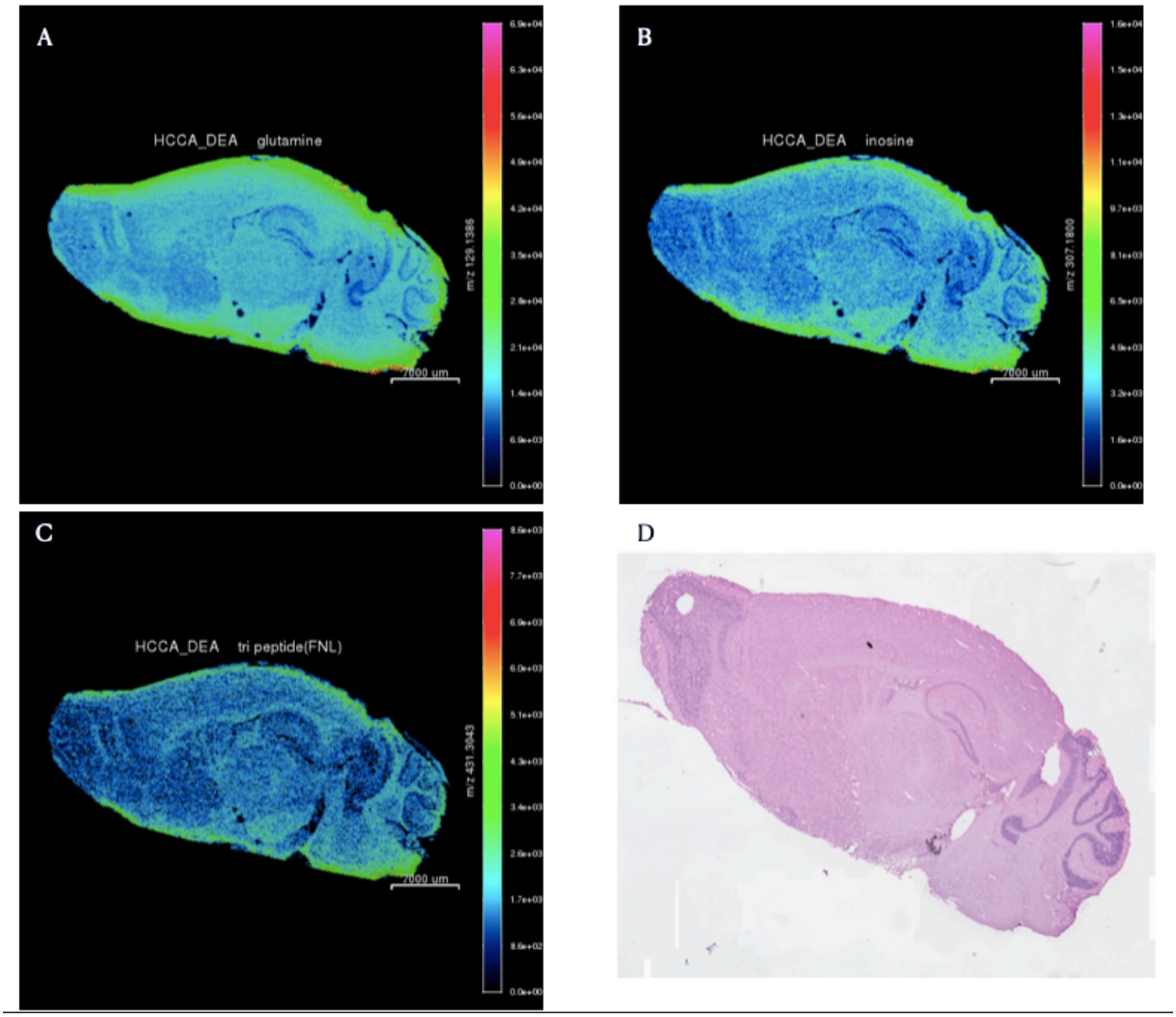

Figure 10: Images representing the intensity of tissue analytes signals detected on brain tissue coated with 10,000 A thickness of HCCA and HCCA-DEA, measured in positive mode; a) intensity of ion m/z 129.1386 (Glutamine); b) intensity of ion m/z 307.1800(Inosine); c) intensity of ion m/z 431.3043 (Tri peptide (FNL)); d) image obtained through a magnifying glass previously stained with H&E stain

In the posterior aspect of the image, a distinct region of the cerebellum is observable. In the central region, the pituitary gland (hypophysis) is prominently depicted. Positioned anteriorly, the olfactory bulb (MOB) is clearly visible.

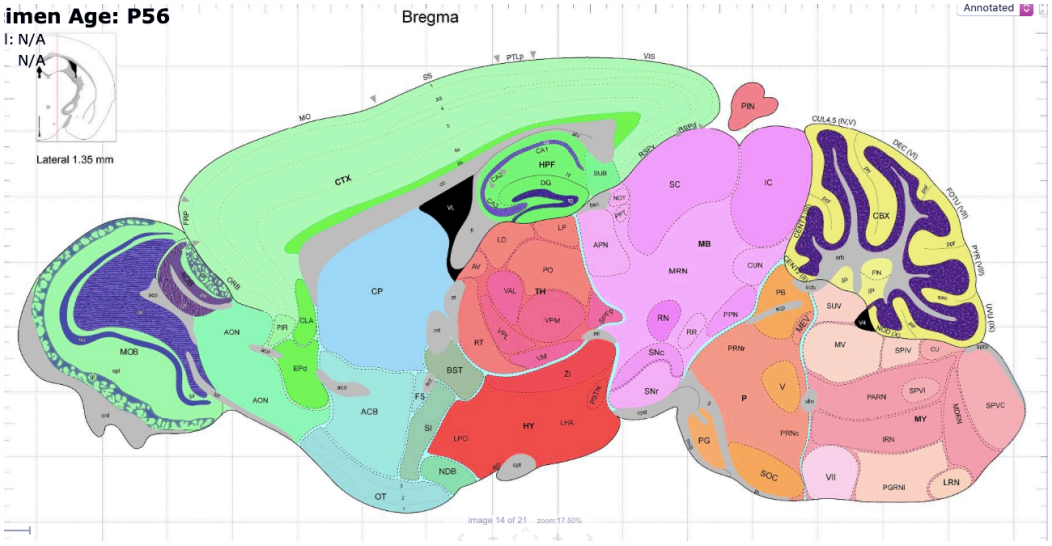

Figure 12: Image that anatomically represents the different regions of the brain, which allows a comparative analysis with images acquired through Rstudio, while identifying and describing the internal structures.[25]

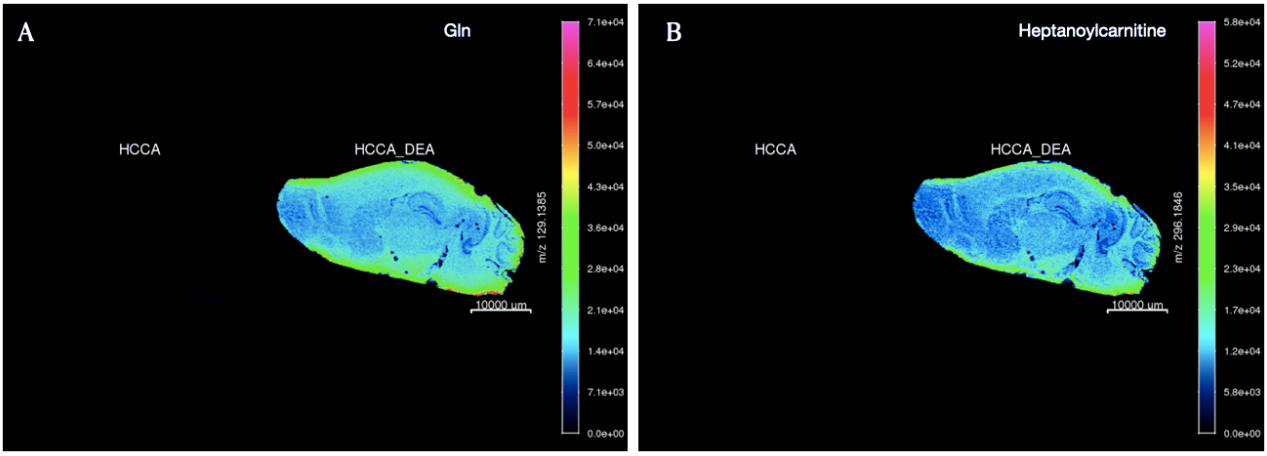

Figure 11: Images representing the intensity of tissue analytes signals detected on brain tissue coated with 10,000 A thickness of HCCA and HCCA-DEA, measured in positive mode compared to conventional matrix ; a) intensity of ion m/z 129.1386 (Glutamine); b) intensity of ion m/z 296.1846 (Heptanoylcarnitine).

When examining brain tissue, it becomes apparent that the α-cyano-4-hydroxycinnamic acid (HCCA) matrix in combination with N,N-Diethylaniline (DEA) yields superior performance compared to other ionic Liquid Matrices (ILMs). Conversely, in pancreatic tissue, these ILMs do not yield desirable outcomes. Specifically, the HCCA-DEA combination produces excellent image quality and enhanced signal intensity for analyte analysis in brain tissue. However, it is important to consider that tissue composition plays a significant role in the selection of the appropriate matrix for optimal results.

4.2.3 MALDI-MSI of pancreas tissue using DHB and DHB-ANI as matrices

4.2.3.1 Analyze of the signal intensity

Upon comparing the conventional matrix (DHB) with the ILMs (DHB+ANI) for pancreatic tissue, it was observed that the use of ILMs led to a noticeable enhancement in intensity.

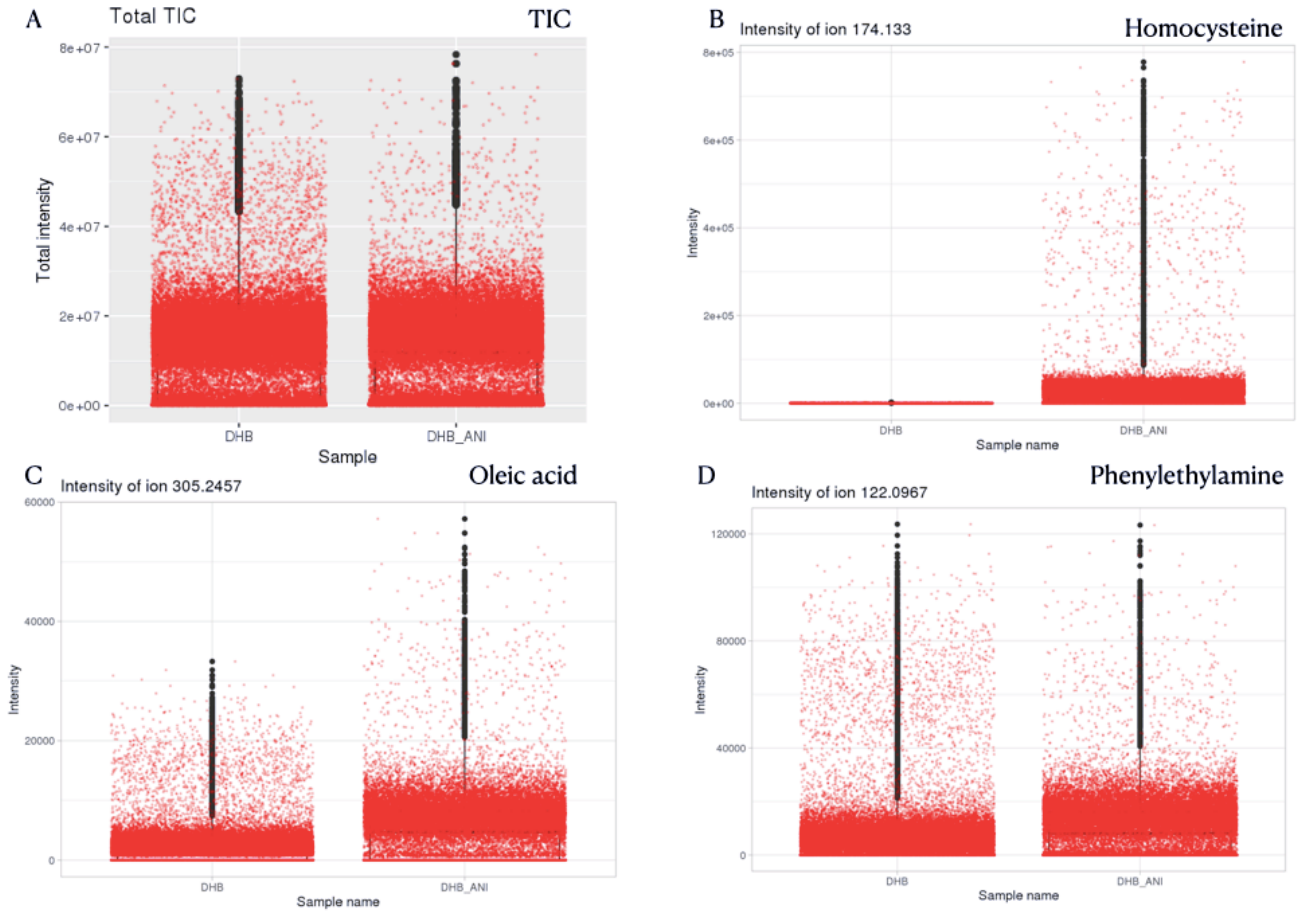

Figure 13: Boxplots representing the intensity of ion signals detected on pancreas tissue coated with 10,000 A thickness of DHB and DHB-ANI, measured in positive mode; a) total ion acount , b) intensity of the analyte m/z 174.133 (Homocysteine), c) intensity of the analyte m/z 305.2475 (Oleic acid) and d) intensity of the analyte m/z 122,0967 (Phenylethylamine)

Figure 13 illustrates a MALDI-MSI comparison depicting the intensity of analyte signals within pancreatic tissue coated with a uniform thickness of 10,000 Å for both ILMs and DHB matrix; (fig. 13a) the TIC plot reveals that the DHB-ANI matrix exhibits higher intensity compared to the DHB matrix.The intensity of the analyte m/z 174.133 (Homocysteine) (Fig. 13b) with the DHB matrix, the analyte exhibits an almost negligible detection signal, whereas it demonstrates a pronounced intensity when utilizing the alternative matrix; intensity of the intensity of the analyte m/z 305.2475 (Oleic acid) (Fig.13c) shows low signal levels when the conventional method is used, comparing the conventional matrix with the ILM we can see an increase in the signal and the intensity of the analyte m/z 122,0967 (Phenylethylamine) (Fig. 13d) demonstrates elevated intensity when subjected to the ILM, while exhibiting lowest levels when utilizing the conventional matrix.

The analyte show in the Figure 13 was selected as the initial test analyte to assess the quantification performance of ILMs in comparison to the previously employed conventional matrix system.

The findings depicted in Figure 13 demonstrate that certain analytes exhibit higher detection intensities when compared to the conventional matrix. Notably, in Figures 13c (analyte m/z 305.2475 (Oleic acid)) and 13d (analyte m/z 122,0967 (Phenylethylamine)), these specific analytes were not detected using the conventional matrix, specifically 2,5-dihydroxybenzoic acid (DHB). This difference in peak detection between the two arrays underscores the greater sensitivity and efficiency of ILM in facilitating the detection of these scans that would otherwise remain undetectable with the conventional array approach.

4.2.3.2 Metabolite identification.

Table 5: Comparison for analytes detected with with ILM and conventional matrix on pancreatic tissue

DHB-ANI		
Ions aducts	**Analytes detected with ILM**	**Analytes detected with DHB**
M+H	28	5
M+Na	14	7
M+K	2	2
M-H_20+H	6	5
Total detected	50	19

Among the various ILMs tested for pancreatic tissue, the DHB+ANI combination exhibited superior performance, enabling the detection of nearly fifty analytes with enhanced accuracy and sensitivity. These analytes are classified into four different ion adduct classes as we can see in table 5.

This table presents the analytes detected in pancreatic tissue using DHB-ANI matrices, in comparison to the use of DHB alone as the matrix. Our findings reveal a significant enhancement in the detection of protonated analytes, with a remarkable increase observed when employing the ILM matrix as compared to the conventional matrix.

In the case of M+N adducts, we observe a relatively less pronounced difference. However, it is noteworthy that the disparity between the two matrices is approximately double, indicating a considerable variation in the detection efficiency between them.

Regarding the last adducts, namely M+K and M-H2O+H, the disparity between the two matrices is deemed negligible.

Upon a comprehensive comparison of both methods, it is evident that the number of metal cation-potassium ion adducts remains consistent between the two matrices. However, in regard to other ion adducts, the ILMs demonstrate a significantly higher detection rate in comparison to the conventional matrix.

When comparing the extended tables present in the annex, the following observations can be made. First, when using ILM, it is possible to detect about ten fatty acids, while with the conventional matrix only one is found. This indicates a significant improvement in the analysis of this analyte family when applying ILM. The same happens with the dipeptides and tripeptides family, where with ILM a total of eleven are found, including the amino acid glutamine (gln), while with the conventional matrix there is approximately half of those detected. In addition, analytes from the family of alkaloids, tryptamines and indoles have been identified through ILM.

On the other hand, using the conventional matrix, it is possible to find analytes of the steroid hormone family, such as vitamin D3, unlike ILM. As for lipids, approximately the same amount is detected in both matrices.

4.2.3.3 Image quality

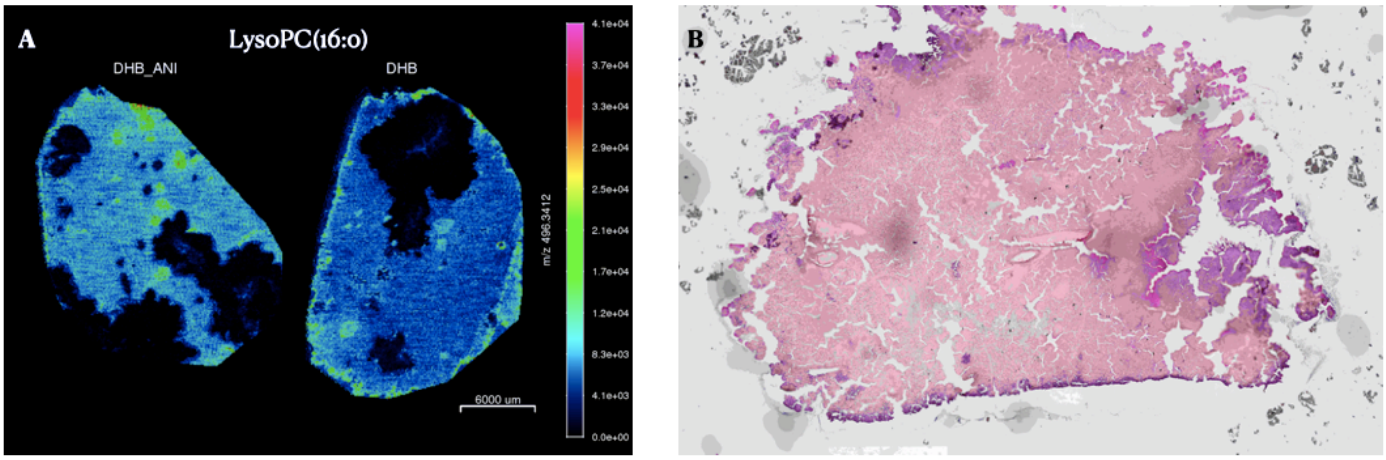

Figure 14: Images representing the intensity of tissue analytes signals detected on pancreas tissue coated with 10,000 A thickness of DHB and DHB-ANI, measured in positive mode; a) intensity of ion m/z 496.3412 (LysoPC(16:0)); b)image obtained through a magnifying glass previously stained with H&E stain

Figure 14 exhibits a comparative assessment of the tissue structure, contrasting the conventional staining method with the tissue image obtained through MALDI-MSI . The analyte m/z 496.3412 (LysoPC(16:0)) (Fig 14a) in the image obtained by MALDI-MSI it is evident that the analyte exhibits significant intensity and a well-defined structural profile compared to the image obtained from the pure crystalline matrix.

Figure 14b presents the H&E staining, which serves as a reference for comparative analysis and guidance.The sample exhibits damage as a result of the staining process.

The pancreas is enveloped by a delicate capsule composed of loose connective tissue. Within the parenchyma, the pancreatic acini and sparsely distributed pancreatic islets are surrounded by a stromal layer of loose connective tissue [24]. Projecting from the capsule into the pancreatic parenchyma, interlobular connective tissue septa effectively organize the tissue into lobules. These interlobular septa serve as housing for interlobular ducts, blood vessels, nerves, and lamellar (Pacinian) corpuscles, which are specialized sensory receptors.[24]

In relation to the anatomical structure of the pancreatic tissue covered by ILMs, conspicuous regions depicted in green coloration are discernibly suggestive of the presence of pancreatic islets. Subsequently, the darkened region observed is likely indicative of the pancreatic duct, as its presence becomes evident upon tissue sectioning, where the incision reveals the presence of the pancreatic duct or intertubular ducts.

In a general sense, the application of DHB plus Aniline demonstrates notable advantages over using DHB alone, as evidenced by various advantageous characteristics. Particularly in the context of pancreatic tissue analysis, the utilization of the DHB+ANI liquid ionic matrix exhibits notable advantages over the traditional method in terms of detecting low molecular weight molecules with enhanced precision, as well as increased abundance and intensity.

5. CONCLUSIONS

This study presents the investigation of six liquid ionic matrices synthesized through the equimolar combination of the crystalline acidic matrices HCCA or DHB with various organic bases.

The experiments conducted using ionizable liquid matrices (ILMs) demonstrated significant advantages over pure crystalline matrices. Our observations revealed that the ILM exhibited a remarkable reduction of over 50% in the intensity of matrix peaks. This reduction, is particularly noticeable when analyzing samples with MALDI MS in the lower range of m/z values, resulted in decreased interference from matrix signals during analyte measurements.

In this study, a wide range of analytes were investigated within the ionizable liquid matrix (ILM) system. These analytes encompassed diverse categories, including low molecular weight compounds such as lipids and amino acids.

ILMs provide remarkable benefits by manifesting the inherent characteristics of their corresponding pure crystalline matrices, allowing for the detection of low molecular weight analytes. These runs exhibit significantly improved signal intensities within the ILM run. Finally, an distinctive attribute observed in ILMs refers to their ability to facilitate the detection of analytes with formation of sodium and potassium adducts. This feature underlines the advantage of ILMs in promoting the generation of stable adduct species involving solid elements and potassium ions during the ionization process.

The objective of this study was to evaluate the capability of ILMs in detecting low molecular weight metabolites while achieving optimal intensity and minimal interference. Our findings demonstrate that utilizing specific combinations of pure crystalline matrices, such as HCCA and DHB, with organic bases, namely DEA and ANI, respectively, on tissues from the pancreas and brain resulted in enhanced signal intensity in MALDI-MS analyses. Notably, this improvement was observed for analytes such as cartidine and cytidine in brain tissue, and for analytes such as phenylethylamine and oleic acid in pancreatic tissue.

Conversely, in our particular case, the acquisition of liquid ionic matrices involves a larger process owing to their synthesis. Furthermore, it is imperative to consider that during matrix deposition, these matrices exhibit higher volatility and heightened sensitivity to temperature variations within the equipment.

In conclusion, this novel technique allows the discovery of a greater number of low molecular weight compounds with a significantly improved intensity and with a reduction of the matrix peaks and, in turn, the reduction of the noise of the metabolite analysis, overcoming some of the limitations of conventional matrices.

6. REFERENCES

7. Walch, A., Rauser, S., Deininger, SO. et al. (2008). MALDI imaging mass spectrometry for direct tissue analysis: a new frontier for molecular histology. Histochem Cell Biol, 130(3), 421-434.
8. Xiaojing Liu, Jason W. Locasale (2017). Metabolomics: A Primer. Trends in Biochemical Sciences, 42(4).
9. Yanes, Ó. (2015). Metabolómica: la ciencia ómica más multidisciplinaria. Sociedad Española de Bioquímica y Biología Molecular, 186, 7-10.
10. Glen L. Hortin (2006). The MALDI-TOF Mass Spectrometric View of the Plasma Proteome and Peptidome. Clinical Chemistry, 52(7), 1223-1237.
11. P. Ràfols, D. Vilalta, J. Brezmes, N. Cañellas, E.D. Castillo, O. Yanes, N. Ramírez, X. Correig (2018). Signal preprocessing, multivariate analysis and software tools for MA(LDI)-TOF mass spectrometry imaging for biological applications. Mass Spectrom. Rev., 37, 281-306.
12. Quan He, Cuirong Sun, Jian Liu, Yuanjiang Pan (2021). MALDI-MSI analysis of cancer drugs: Significance, advances, and applications. TrAC Trends in Analytical Chemistry, 136, 116183.
13. McDonnell, L.A., Römpp, A., Balluff, B. et al. (2015). Discussion point: reporting guidelines for mass spectrometry imaging. Anal Bioanal Chem, 407(8), 2035-2045.
14. Kaspar, S., Peukert, M., Svatos, A., Matros, A. and Mock, H.-P. (2011). MALDI-imaging mass spectrometry – An emerging technique in plant biology. Proteomics, 11(9), 1840-1850.
15. Stephen Castellino, M Reid Groseclose & David Wagner (2011). MALDI imaging mass spectrometry: bridging biology and chemistry in drug development. BIOANALYSIS, 3(21).
16. Tatiana C. Rohner, Dieter Staab, Markus Stoeckli (2005). MALDI mass spectrometric imaging of biological tissue sections. Mechanisms of Ageing and Development, 126(1).
17. Roman A. Zubarev and Alexander Makarov (2013). Analytical Orbitrap Mass Spectrometry. Chemistry, 85(11), 5288-5296.
18. MORENO, G., R. GALÁN, B. PÉREZ & J.M. SANZ-ANQUELA (2019). Caracterización de Amanita phalloides y Lepiota brunneoincarnata mediante MALDI-TOF en la intoxicación ciclopeptídica. Bol. Soc. Micol. Madrid, 43, 191–201.
19. Robert L. Caldwell, Richard M. Caprioli (2005). Tissue Profiling by Mass Spectrometry: A Review of Methodology and Applications. Molecular & Cellular Proteomics, 4(4).
20. Ying L. Li, Michael L. Gross (2004). Ionic-liquid matrices for quantitative analysis by MALDI-TOF mass spectrometry. Journal of the American Society for Mass Spectrometry, 15(12), 1833-1837.
21. Ke Huang, Xiaotong Zhang, Daniel W. Armstrong (2010). Ionic cyclodextrins in ionic liquid matrices as chiral stationary phases for gas chromatography. Journal of Chromatography A, 1217(32), 5261-5273.
22. Almas Bashir, Tahir Iqbal Awan, Aqsa Tehseen, Muhammad Bilal Tahir, Mohsin Ijaz (2020). Interfaces and surfaces. In Chemistry of Nanomaterials, Chapter 3. Elsevier.
23. Ke Huang, Xiaotong Zhang, Daniel W. Armstrong (2010). Ionic cyclodextrins in ionic liquid matrices as chiral stationary phases for gas chromatography. Journal of Chromatography A, 1217(32), 5261-5273.
24. Tholey, A., Heinzle, E. (2006). Ionic (liquid) matrices for matrix-assisted laser desorption/ionization mass spectrometry—applications and perspectives. Anal Bioanal Chem, 386(1), 24-37.
25. Armstrong DW, Zhang LK, He L, Gross ML. (2001). Ionic liquids as matrixes for matrix-assisted laser desorption/ionization mass spectrometry. Anal Chem, 73(15), 3679-3686.

26. Abdelhamid HN. (2018). Ionic Liquid-Assisted Laser Desorption/Ionization–Mass Spectrometry: Matrices, Microextraction, and Separation. Methods and Protocols, 1(2), 23.

27. Almas Bashir, Tahir Iqbal Awan, Aqsa Tehseen, Muhammad Bilal Tahir, Mohsin Ijaz (2020). Interfaces and surfaces. In Chemistry of Nanomaterials, Chapter 3. Elsevier.

28. Raul Calavia, Fatima E. Annanouch, Xavier Correig, Oscar Yanes (2012). Nanostructure Initiator Mass Spectrometry for tissue imaging in metabolomics: Future prospects and perspectives. Journal of Proteomics, 75(16), 5061-5068.

29. F. Lévy (2016). Film Growth and Epitaxy: Methods. In Reference Module in Materials Science and Materials Engineering. Elsevier.

30. Atlas thumbnails : Allen brain atlas: Mouse brain. (s/f). Brain-map.org. Recuperado el 10 de junio de 2023, de https://mouse.brain-map.org/experiment/thumbnails/100142144?image_type=atlas

31. Endocrine pancreas. (s/f). Histologyguide.com. Recuperado el 10 de junio de 2023, de https://www.histologyguide.com/slideview/MH-131-pancreas/13-slide-1.html?x=71096&y=39386&z=47.0

Annex

Brain tissue

	HCCA-DEA			HCCA		
	m/z	**Ion adduct**	**Compound name**	**m/z**	**Ion adduct**	**Compound name**
1	132,0771	Prot	Creatine	116,0705	Prot	Proline
2	160,1337	Prot	5-aminovaleric acid betaine	132,0706	Prot	Creatine
3	162,1130	Prot	carnitine	165,0504	Prot	2-Hydroxycinnamic acid
4	184,0739	Prot	Phosphocholine	184,0731	Prot	phosphocholine
5	258,1109	Prot	glycerophosphoryl-choline	192,0653	Prot	5-Hydroxyindoleacetic-acid
6	400,3413	Prot	Hexadecanoylcaritine	205,0969	Prot	tryptophan
7	426,3589	Prot	Octadecenoylcarnitine	391,2837	Prot	Hydroxy-oxo-cholanoic acid
8	496,3413	Prot	lysoPC(16:0)	419,3149	Prot	110-Carboxy-alpha-chromanol
9	524,3725	Prot	lysoPC(18:0)	496,3390	Prot	Hexadecyl ferulate
10	146,9822	Sodiat	Phosphonoacetaldehyde	150,0911	Dehyd	S-methylmethionine
11	206,0559	Sodiat	Phosphocholine	205,0969	Dehyd	Met-Ala
12	227,0795	Sodiat	Tryptophan	233,1279	Dehyd	Met Val
13	280,0929	Sodiat	glycerophosphoryl-choline	192,0653	Prot	5-Hydroxyindoleacetic-acid
14	296,1847	Sodiat	Heptanoylcarnitine	297,1257	Prot	MF
15	329,1741	Sodiat	50-carbocy-gamma-charo-manol	316,1624	Sodiat	KF
16	330,0730	Sodiat	glutathione	233,1272	Dehyd	VM
17	396,2361	Sodiat	Dodecanedioylcarnitine C1-DC			
18	282,1860	Potas	Cytidine			
19	301,1429	Potas	Sorbitol 6-phosphate			
20	538,3957	Potas	Taurodeoxycholic acid			
21	173,116	Dehyd	Azelaic acid			
22	295,1296	Prot	FE			
23	297,1271	Prot	MF			
24	129,1386	Prot	gln			
25	335,1349	Sodiat	FF			

Pancreatic tissue-1

	DHB			DHB-ANI		
	m/z	**Ion adduct**	**Compound name**	**m/z**	**Ion adduct**	**Compound name**
1	258,1103	Prot	Glycerophosphoryl-choline	118,0654	Prot	Indole
2	307,1619	Prot	Acetylcarnitine C2	122,0967	Prot	Phenylethylamine
3	349,0564	Prot	Inosinmonophosphat	130,0654	Prot	Isoamyl isothiocyanate
4	544,3372	Prot	lysoPC(20:4)	132,0770	Prot	Creatinie
5	131,0484	Sodiat	p-Cresol	161,1077	Prot	Tryptamine
6	138,0300	Sodiat	3-Keto-2-methylbutyrate	180,0659	Prot	Hippuric Acid
7	192,9887	Sodiat	Dihydroxyacetone phosphate	182,0815	Prot	tyrosine
8	544,3372	Sodiat	lysoPC(18:1)	184,0737	Prot	Phosphocholine
9	156,1571	Potas	Indole	190,1867	Prot	3-indolepropionic acid
10	285,0937	Dhyd	Dimethyl fukiic acid	198,1120	Prot	methanaphrine
11	396,3494	Dhyd	Desmosterol, vitamin D3	203,2235	Prot	Spermine
12	400,3396	Dhyd	Hydroxyhexadecanoylcaritine	249,1266	Prot	Met Val
13	426,3550	Dhyd	Hydroxyoctadecenoylcarnitine	258,1122	Prot	Glycerophosphoryl-choline
14	478,3255	Dhyd	lysoPC(16:1)	307,1643	Prot	Acetylcarnite C2
15	306,1578	Prot	RM	371,3159	Prot	Diethylhexyl adipate
16	316,1615	Sodiat	KF	391,2850	Prot	Hydroxy-oxo-cholanoic acid
17	316,1615	Sodiat	FK	400,3432	Prot	Hecadecanoylcarnitine
18	282,1785	Sodiat	KL	419,3162	Prot	Hecadecy ferulate
19	403,3086	Potas	FAK	426,3588	Prot	Octadecenoylcaritine
20				496,3407	Prot	lysoPC(16:0)
21				520,3407	Prot	lysoPC(18:0)
22				522,3560	Prot	lysoPC(18:1)
23				524,3719	Prot	lysoPC(18:0)
24				546,3559	Prot	lysoPC(20:3)
25				156,0423	Sodiat	Indoxyl

Pancreatic tissue-2

	DHB			DHB-ANI		
	m/z	**Ion adduct**	**Compound name**	**m/z**	**Ion adduct**	**Compound name**
26				169,0478	Sodiat	Adapic acid
27				206,0557	Sodiat	phosphocholine
28				296,1103	Sodiat	Glutaconylcarnitine C5:1-DC
29				305,2457	Sodiat	Oleic acid
30				413,2671	Sodiat	Hydroxy-oxo-cholanoic acid
31				441,2982	Sodiat	110-carboxy-alpha-chromanol
32				518,3228	Sodiat	lysoPC(16:0)
33				542,3226	Sodiat	lysoPC(18:2)
34				546,3535	Sodiat	lysoPC(18:0)
35				566,3227	Sodiat	lysoPC(20:4)
36				151,1254	Potas	Uracil
37				174,1330	Potas	homocysteine
38				122,0923	Dhyd	Tyraminde
39				415,1915	Dhyd	Glu trp pro
40				146,1651	Prot	Spermidine
41				249,1266	Prot	VM
42				297,1266	Prot	MF
43				129,1389	Prot	gln
44				413,1881	Sodiat	DKF
45				316,1642	Sodiat	FK
46				432.1945	Sodiat	MFL
47				393,2077	Dhyd	DKF
48				314,1650	Dhyd	DPV
49				420,2314	Dhyd	NFR
50				366,1609	Dhyd	ESF

list_of_NTs_metb

mz_theo	formula	compound	class
174.1116	C6H14N4O2	"arginine"	"amino acid"
167.0946	C9H13NO2	"3-Methoxytyramine"	"NTs and metabolites"
211.0844	C10H13NO4	"3-O-Methyl-DOPA"	"NTs and metabolites"
191.0582	C10H9NO3	"5-Hydroxyindoleacetic-acid"	"NTs and metabolites"
175.0633	C10H9NO2	"5-hydroxyindole-acetaldehyde"	"NTs and metabolites"
176.0949	C10H12N2O	"Serotonin"	"NTs and metabolites"
177.07898	C10H11NO2	"5-Hydroxy-Tryptophol"	"NTs and metabolites"
220.08479	C11H12N2O3	"5-hydroxytryptophan"	"NTs and metabolites"
248.11609	C13H16N2O3	"6-hydroxymelatonin"	"NTs and metabolites"
130.12184	C5H14N4	"Agmatine"	"NTs and metabolites"
130.12184	C4H7N3O	"Creatinine"	"NTs and metabolites"
121.01974	C3H7NO2S	"Cysteine"	"amino acid"
153.078979	C8H11NO2	"Dopamine"	"NTs and metabolites"
168.04225	C8H8O4	"3,4-Dihydroxyphenylacetic-acid(DOPAC)"	"NTs and metabolites"
152.047348	C8H8O3	"Dihydroxyphenyl-Acetaldehyde(DOPAL)"	"NTs and metabolites"
182.0579	C9H10O4	"Homovanillic-acid(HVA)"	"NTs and metabolites"
197.0688	C9H11NO4	"Levodopa(L-DOPA)"	"NTs and metabolites"
169.073898	C8H11NO3	"Norepinephrine"	"NTs and metabolites"
170.0579	C8H10O	"Dihydroxyphenylglycol(DOPEG)"	"NTs and metabolites"
183.0895	C9H13NO3	"Epinephrine"	"NTs and metabolites"
174.06405	C6H10N2O4	"Formiminoglutamic-Acid"	"NTs and metabolites"
103.0633	C4H9NO2	"gamma-Aminobutyric-acid(GABA)"	"NTs and metabolites"
111.0796	C5H9N3	"Histamine"	"NTs and metabolites"
155.06947	C6H9N3O2	"Histidine"	"NTs and metabolites"
146.1055	C6H14N2O2	"Lysine"	"NTs and metabolites"
197.10519	C10H15NO3	"Metanephrine"	"NTs and metabolites"
166.06298	C9H10O3	"MOPAL"	"NTs and metabolites"
184.07356	C9H12O4	"MOPEG"	"NTs and metabolites"
88.10004	C4H12N2	"putrescine"	"NTs and metabolites"
145.15789	C7H19N3	"spermidine"	"NTs and metabolites"
125.01466	C2H7NO3S	"Taurine"	"NTs and metabolites"
212.06846	C10H12O5	"vanillactic-acid"	"NTs and metabolites"
210.05282	C10H10O5	"Vanilpyruvic-acid"	"NTs and metabolites"
198.05282	C9H10O5	"Vanillyl mandelic acid(VMA)"	"NTs and metabolites"

list_peptides_amino_acids_1

mz_theo	formula	name	class
226.10576	227.1137	AH	di/tri peptides
188.11536	189.1233	VA	di/tri peptides
218.12586	219.1338	VT	di/tri peptides
360.16346	361.1714	VDE	di/tri peptides
287.19476	288.2027	RL	di/tri peptides
260.13646	261.1444	LE	di/tri peptides
216.14676	217.1547	VV	di/tri peptides
293.13706	294145	FQ	di/tri peptides
293.17286	294.1808	KF	di/tri peptides
294.12066	295.1286	FE	di/tri peptides
248.11866	249.1266	VM	di/tri peptides
218.12606	219134	SL	di/tri peptides
245.13716	246.1451	NL	di/tri peptides
259.15196	260.1599	QL	di/tri peptides
232.14126	233.1492	TL	di/tri peptides
188.11556	189.1235	GL	di/tri peptides
399.18956	400.1975	FPH	di/tri peptides
358.25686	359.2648	KVL	di/tri peptides
303.14186	304.1498	GDL	di/tri peptides
333.15206	334.16	SDL	di/tri peptides
252.10956	253.1175	SF	di/tri peptides
347.16846	348.1764	SEL	di/tri peptides
230.16226	231.1702	VL	di/tri peptides
363.17856	364.1865	FPT	di/tri peptides
275.12586	276.1338	AW	di/tri peptides
331.21006	332218	TVL	di/tri peptides
301.19946	302.2074	LGL	di/tri peptides
301.14156	302.1495	PW	di/tri peptides
244.17766	245.1856	LL	di/tri peptides
464.20486	465.2128	YPW	di/tri peptides
160.08406	161092	AA	di/tri peptides
346.16406	347172	AAW	di/tri peptides
218.08996	219.0979	AE	di/tri peptides
347.13166	348.1396	AEE	di/tri peptides

list_peptides_amino_acids_1-1

mz_theo	formula	name	class
236.11516	237.1231	AF	di/tri peptides
217.14186	218.1498	AK	di/tri peptides
330.22596	331.2339	AKL	di/tri peptides
202.13156	203.1395	AL	di/tri peptides
331.17336	332.1813	ALE	di/tri peptides
302.15836	303.1663	ANV	di/tri peptides
245.14796	246.1559	AR	di/tri peptides
319.15546	320.1634	AVM	di/tri peptides
317.15766	318.1656	DAL	di/tri peptides
408.19976	409.2077	DKF	di/tri peptides
246.12076	247.1287	DL	di/tri peptides
383.17886	384.1868	DLH	di/tri peptides
329.15766	330.1656	DPV	di/tri peptides
374.17926	375.1872	DQL	di/tri peptides
331.17356	332.1815	EAL	di/tri peptides
275.14696	276.1549	EK	di/tri peptides
260.13666	261.1446	EL	di/tri peptides
236.11516	237.1231	FA	di/tri peptides
312.14626	313.1542	FF	di/tri peptides
441.18906	442197	FFE	di/tri peptides
222.09926	223.1072	FG	di/tri peptides
293.17326	294.1812	FK	di/tri peptides
278.16216	279.1701	FL	di/tri peptides
349.19926	350.2072	FLA	di/tri peptides
335.18326	336.1912	FLG	di/tri peptides
279.12096	280.1289	FN	di/tri peptides
392.20466	393.2126	FNL	di/tri peptides
262.13076	263.1387	FP	di/tri peptides
421.23106	422239	FQK	di/tri peptides
212.09006	213098	GH	di/tri peptides
325.17416	326.1821	GHL	di/tri peptides
203.12616	204.1341	GK	di/tri peptides
331.22086	332.2288	GKK	di/tri peptides
206.07196	207.0799	GM	di/tri peptides

list_peptides_amino_acids_1-2

mz_theo	formula	name	class
323.14776	324.1557	GTF	di/tri peptides
174.09956	175.1075	GV	di/tri peptides
363.16426	364.1722	HAH	di/tri peptides
302.13686	303.1448	HF	di/tri peptides
292.12766	293.1356	HH	di/tri peptides
283.16336	284.1713	HK	di/tri peptides
268.15256	269.1605	HL	di/tri peptides
355.18396	356.1919	HLS	di/tri peptides
252.12136	253.1293	HP	di/tri peptides
406.25696	407.2649	KFL	di/tri peptides
396.24746	397.2554	KHL	di/tri peptides
259.18876	260.1967	KL	di/tri peptides
372.27266	373.2806	KLL	di/tri peptides
247.15236	248.1603	KT	di/tri peptides
344.24146	345.2494	KVV	di/tri peptides
309.16796	310.1759	KY	di/tri peptides
273.16816	274.1761	LAA	di/tri peptides
339.18976	340.1977	LAH	di/tri peptides
315.21466	316.2226	LAL	di/tri peptides
374.21596	375.2239	LDK	di/tri peptides
325.17416	326.1821	LGH	di/tri peptides
344.21626	345.2242	LGR	di/tri peptides
367.22116	368.2291	LHV	di/tri peptides
316.21036	317.2183	LKG	di/tri peptides
343.24626	344.2542	LLV	di/tri peptides
228.14666	229.1546	LP	di/tri peptides
285.16786	286.1758	LPG	di/tri peptides
259.15266	260.1606	LQ	di/tri peptides
386.26286	387.2708	LRV	di/tri peptides
317.17306	318181	LW	di/tri peptides
296.11826	297.1262	MF	di/tri peptides
409.20296	410.2109	MFL	di/tri peptides
316.17426	317.1822	NAL	di/tri peptides
279.12116	280.1291	NF	di/tri peptides

list_peptides_amino_acids_1-3

mz_theo	formula	name	class
373.23196	374.2399	NLK	di/tri peptides
359.21606	360224	NVK	di/tri peptides
230.08946	231.0974	PD	di/tri peptides
244.10496	245.1129	PE	di/tri peptides
342.22576	343.2337	PKV	di/tri peptides
202.09426	203.1022	PS	di/tri peptides
216.11046	217.1184	PT	di/tri peptides
214.13096	215.1389	PV	di/tri peptides
274.16386	275.1718	QK	di/tri peptides
380.16906	381177	QSF	di/tri peptides
373.23186	374.2398	QVK	di/tri peptides
321.17936	322.1873	RF	di/tri peptides
468.24736	469.2553	RFF	di/tri peptides
400.27896	401.2869	RLL	di/tri peptides
305.15116	306.1591	RM	di/tri peptides
289.16286	290.1708	SAL	di/tri peptides
242.10066	243.1086	SH	di/tri peptides
266.12596	267.1339	TF	di/tri peptides
303.17836	304.1863	TLA	di/tri peptides
247.11576	248.1237	TQ	di/tri peptides
282.12096	283.1289	TY	di/tri peptides
254.13696	255.1449	VH	di/tri peptides
245.17326	246.1812	VK	di/tri peptides
287.18406	288192	VLG	di/tri peptides
358.22066	359.2286	VLQ	di/tri peptides
317.19396	318.2019	VLS	di/tri peptides
231.12096	232.1289	VN	di/tri peptides
378.18996	379.1979	VNF	di/tri peptides
331.20976	332.2177	VTL	di/tri peptides
287.18326	288.1912	VVA	di/tri peptides
329.23036	330.2383	VVL	di/tri peptides
280.14136	281.1493	VY	di/tri peptides
377.19436	378.2023	VYP	di/tri peptides
261.11086	262.1188	WG	di/tri peptides

list_peptides_amino_acids_1-4

mz_theo	formula	name	class
328.14166	329.1496	YF	di/tri peptides
425.19336	426.2013	YFP	di/tri peptides
318.13226	319.1402	YH	di/tri peptides
278.12576	279.1337	YP	di/tri peptides
337.17386	338.1818	YR	di/tri peptides
354.20066	355.2086	AHK	di/tri peptides
434.19326	435.2012	ERM	di/tri peptides
381.15286	382.1608	ESF	di/tri peptides
364.20996	365.2179	FAK	di/tri peptides
231.13216	232.1401	GR	di/tri peptides
204.11046	205.1184	SV	di/tri peptides
71.03711	C3H5ON	Ala	amino acid
156.10111	C6H12ON4	arg	amino acid
114.04293	C4H6O2N2	asn	amino acid
115.0886	C4H5O3N	asp	amino acid
103.00919	C3H5ONS	cys	amino acid
129.1155	C5H7O3N	glu	amino acid
128.1307	C5H8O2N2	gln	amino acid
57.0519	C2H3ON	gly	amino acid
137.1411	C6H7ON3	his	amino acid
113.1594	C6H11ON	ils/leu	amino acid
128.1741	C6H12ON2	lys	amino acid
131.1926	C5H9ONS	met	amino acid
147.1766	C9H9ON	phe	amino acid
97.1167	C5H7ON	pro	amino acid
87.0782	C3H5O2N	ser	amino acid
101.1051	C4H7O2N	thr	amino acid
186.2132	C11H10ON2	trp	amino acid
163176	C9H9O2N	tyr	amino acid
99.1326	C5H9ON	val	amino acid
407.21626	408.2242	NFK	di/tri peptides
435.22176	436.2297	NFR	di/tri peptides
389.20576	390.2137	WHK	di/tri peptides

simply_list_small_molec

mz_theo	formula	compd	classification
58.005	CH_3COOH	Acetatic acid	Organic Acids
75.032		glycine	
88.016	C3H4O3	Pyruvic Acid	Organic Acids
88.052	C3H7COOH	butyric acid	fatty acids
88.100	C4H12N2	putrescine	alkaloids
88.100	C4H12N2	putrescine	alkaloids
89.011	C2H3NO3	oxamic acid	others
89.048	C3H7NO2	Sarcosine	Biogenic Amines
89.048	C3H7NO2	Beta-alanine	Amino acids
89.048	C3H7NO2	alanine	amino acids
89.084	C4H11NO	Dimethylethanolamine	
90.032	C3H6O3	Lactic Acid	Organic Acids
92.047	C3H8O3	Glycerol	
103.040	C4H7O3	3-hydroxybutyric acid	Organic Acids
103.063	C4H9NO2	beta-Aminobutyric acid	Amino acid related
103.063	C4H9NO2	γ-aminobutyric acid (GABA)	NT
103.063	C4H9NO2	γ-aminobutyric acid (GABA)	NT
103.063	C4H9NO2	γ-aminobutyric acid (GABA)	NT
104.047	C4H8O3	Ethoxyacetic acid	
104.108	C5H14NO	Choline	Vitamines and Cofactors
104.108	C5H14NO	choline	others
105.043	C3H7NO3	serine	amino acids
106.027	C3H6O4	glyceric acid	organic acids
108.042	C3H8O4	2,2-Dihydroperoxypropane	
108.058	C7H8O	p-Cresol	
109.020	C2H7NO2S	hypotaurine	others
111.043	C4H5N3O	cytosine	others
111.043	C4H5N3O	cytosine	others
111.080	C5H9N3	Histamine	Biogenic Amines
112.027	C4H4N2O2	uracil	pyrimidine
112.027	C4H4N2O2	Uracil	pyrimidine
113.059	C4H7N3O	creatinine	others
113.059		creatinine / pyroglutamic acid	
113.059	C4H7N3O	creatinine	others

simply_list_small_molec-1

115.040	C5H7O3	3-Keto-2-methylbutyrate	
115.063	C5H9NO2	proline	amino acids
116.011	C4H4O4	fumaric acid	organic acids
116.047	C5H8O3	Glutarate semialdehyde	
116.047	C5H8O3	levulinic acid	organic acids
116.095	C5H12N2O	aminopentanamide	others
117.058	C8H7N	Indole	Indoles and Derivates
117.079	C5H11NO2	5-Aminovaleric acid	Amino acid related
117.079	C5H11NO2	Betaine	
117.079	C5H11NO2	Valine	amino acids
118.027	C4H6O4	succinic acid	organic acids
118.027	C4H6O4	succinic acid	organic acids
118.027		succinic acid	
119.058	C4H9NO3	threonine	amino acids
119.058	C4H9NO3	threonine	amino acids
119.059		threonine	
121.020	C3H7NO2S	cysteine	amino acids
121.020	C3H7NO2S	cysteine	amino acids
121.089	C8H11N	Phenylethylamine	Biogenic amines
122.048	C6H6N2O	nicotinamide	alkaloids
122.048	C6H6N2O	nicotinamide	alkaloids
123.993	C2H5O4P	phosphonoacetaldehyde	others
123.993	C2H5O4P	phosphonoacetaldehyde	others
123.993		phosphonoacetaldehyde	
123.993		phosphonoacetaldehyde	
125.015	C2H7NO3S	taurine	others
125.015		taurine	
125.981	C2H6O2S2	Methyl methanethiosulfonate	
125.999	C2H6O4S	isethionic acid	others
128.059	C5H8N2O2	2-amino-4-cyanobutanoic	amino acids
129.043	C5H7NO3	pyroglutamic acid	amino acids
129.043		pyroglutamic acid	
129.058		Isoamyl isothiocyanate	
129.061	C6H11NS	Isoamyl isothiocyanate	
129.079	C6H11NO2	pipecolic acid	others

simply_list_small_molec-2

130.027	C5H6O4	citraconic acid	organic acids
130.027	C5H6O4	citraconic acid	organic acids
130.063	C6H10O3	5-oxohexanoic acid	fatty acids
131.058	C5H9NO3	Trans-hydroxyproline	Biogenic Amines
131.069	C4H9N3O2	creatine	amino acids
131.069	C4H9N3O2	creatine	amino acids
131.069	C4H9N3O2	creatine	amino acids
131.095	C6H13NO2	Leucine	Amino acids
131.095	C6H13NO2	Isoleucine	Amino acids
131.095		Leucine	
132.090	C5H12N2O2	Ornithine	Amino acids
132.090	C5H12N2O2	ornithine	amino acids
132.090		ornithine	
132.097	C7H16S	Heptanethiol	
133.038	C4H7NO4	aspartic acid	amino acids
133.038	C4H7NO4	aspartic acid	amino acids
133.038		aspartic acid	
133.053	C8H7NO	Indoxyl	Indoles and Derivates
133.074	C5H11NO3	L-Aspartate-semialdehyde	
134.022	C4H6O5	Malic acid	
134.022	C4H6O5	malic acid	organic acids
134.022	C4H6O5	Malic acid	
134.022		Malic acid	
135.035	C4H9NO2S	Homocysteine	Amino acid related
135.055	C5H5N5	adenine	purine
135.055	C5H5N5	adenine	purine
136.037	C4H8O5	threonic acid	organic acids
136.037		threonic acid	
136.037		threonic acid	
136.038		threonic acid	
136.039	C5H4N4O	purine	
136.039	C5H4N4O	hypoxanthine	purine
136.039	C5H4N4O	hypoxanthine	purine
136.039		hypoxanthine	
136.052	C8H8O2	4-Hydroxyphenylacetaldehyde	

simply_list_small_molec-3

137.084	C8H11NO	tyramine	
141.079	C7H11NO2	arecaidine	alkaloids
142.074	C6H10N2O2	ectoine	others
143.095	C7H13NO2	Proline betaine	
145.158	C7H19N3	spermidine	alkaloids
145.158	C7H19N3	spermidine	alkaloids
145.158	C7H19N3	spermidine	alkaloids
146.058	C6H10O4	Adapic acid	
146.069	C5H10N2O3	glutamine	amino acids
146.069	C5H10N2O3	glutamine	amino acids
146.118	C7H16NO2	acetylcholine	
147.053	C5H9NO4	glutamic acid	amino acids
147.053	C5H9NO4	glutamic acid	amino acids
147.054		glutamic acid	
147.090	C6H13NO3	2-Amino-4-hydroxy-3-methylpentanoic acid	
148.052	C9H8O2	cinnamic acid	organic acids
149.051	C5H11NO2S	methionine	amino acids
149.051	C5H11NO2S	methionine	amino acids
149.981	C4H6O2S2	Asparagusic acid	
150.068	C9H10O2	3-phenylpropionic acid	organic acids
153.079	C8H11NO2	dopamine	NT
153.090	C7H11N3O	N-acetylhistamine	
154.099	C9H14O2	2-Nonenoic acid gamma-lactone	
155.069	C6H9N3O2	histidine	amino acids
157.038	C6H7NO4	amino-muconic acid	amino acids
158.131	C9H18O2	Pelargonic acid	
159.126	C8H17NO2	5-Aminovaleric acid betaine	
159.126	C8H17NO2	amino-octanoic acid	amino acids
160.074	C7H12O4	Pimelic acid	STD
160.074	C7H12O4	Pimelic acid	STD
160.100	C10H12N2	tryptamine	
160.134	C8H18NO2	Propionylcholine	
161.069	C6H11NO4	Alpha-aminoadipic acid	Organic Acids
161.105	C7H15NO3	carnitine	others
162.113	C7H16NO3	Carnitine C0	Acylcarnitines

simply_list_small_molec-4

164.033	C6H4N4O2	lumazine	others
164.047	C9H8O3	2-Hydroxycinnamic acid	
165.046	C5H11NO3S	Methionine-sulfoxide	Biogenic Amines
165.079	C9H11NO2	phenylalanine	amino acids
165.079		phenylalanine	
165.079	C9H11NO2	phenylalanine	amino acids
165.082	C6H15NO2S	S-methylmethionine	others
167.058	C8H9NO3	pyridoxal	
169.074	C8H11NO3	norepinephrine	NT
169.085	C7H11N3O2	Methylhistidine	
169.998	C3H7O6P	dihydroxyacetone phosphate	others
169.999		dihydroxyacetone phosphate	
172.074	C8H12O4	octenedioic acid	
172.110	C9H16O3	Tetrahydrofurfuryl butyrate	
172.183	C11H24O	Undecanol	
174.016	C6H6O6	aconitic acid	organic acids
174.016	C6H6O6	aconitic acid	organic acids
174.100	C7H14N2O3	Acetyl-ornithine	Biogenic Amines
174.112	C6H14N4O2	arginine	amino acids
174.112	C6H14N4O2	arginine	amino acids
175.048	C6H9NO5	N-acetylaspartic acid	others
175.063	C10H9NO2	3-Indoleacetic acid	Indoles and Derivates
175.096	C6H13N3O3	Citrulline	Amino acids
175.096		Citrulline / amino-octanoic acid	
175.096		Citrulline	
176.032	C6H8O6	Ascorbic acid (Vitamin C)	Organic Acids
176.095	C10H12N2O	serotonin	
176.095		serotonin	
179.058	C9H9NO3	Hippuric Acid	Carboxylic acids
180.053	C8H8N2O3	Nicotinic acid	Organic Acids
180.063	C6H12O6	myo-inositol	others
180.063	C6H12O6	Glucose	
180.063		Glucose	
180.063		Glucose	
180.063	C6H12O6	myo-inositol	others

simply_list_small_molec-5

180.064	C6H12O6	myo-inositol / Glucose	
181.074	C9H11NO3	tyrosine	amino acids
181.074		tyrosine	
182.044	C6H6N4O3	Methyluric acid	
182.058	C9H10O4	homovanillic acid	
182.058		homovanillic acid	
183.066	C5H14NO4P	phosphocholine	others
183.066		phosphocholine	
183.066		phosphocholine	
183.090	C9H13NO3	epinephrine	NT
183.090	C9H13NO3	epinephrine	NT
184.074	C9H12O4	3-methoxy-4-hydroxyphenylglycol	others
184.074	C9H12O4	3-methoxy-4-hydroxyphenylglycol	others
184.074	C5H15NO4P	O-phosphocholine	
186.120		3-Oxodecanoic acid	
186.126	C10H18O3	3-Oxodecanoic acid	
186.126		3-Oxodecanoic acid	
186.126		3-Oxodecanoic acid	
188.014	C7H8O4S	p-Cresol sulfate	
188.105	C9H16O4	Azelaic acid	STD
188.105	C9H16O4	Azelaic acid	STD
188.108		Azelaic acid	
188.127	C7H16N4O2	Homoarginine	Amino acid related
189.064	C7H11NO5	N-acetylglutamic acid	others
189.079	C11H11NO2	3-Indolepropionic acid	Indoles and Derivates
190.066	C8H14O3S	Ethyl 4-(acetylthio) butyrate	
191.058	C10H9NO3	5-hydroxyindoleacetic acid	others
192.027	C6H8O7	citric acid	
192.057	C6H12N2O3S	Cys-Ala	
193.074	C10H11NO3	3-Methylhippuric acid	STD
193.074	C10H11NO3	3-Methylhippuric acid	STD
193.074	C10H11NO3	3-Methylhippuric acid	STD
193.074	C10H11NO3	Phenylacetylglycine	
194.043	C6H10O7	glucuronic acid	organic acids
196.121	C10H16N2O2	L-alpha-Amino-1H-pyrrole-1-hexanoic acid	

simply_list_small_molec-6

197.069	C9H11NO4	Dihydroxyphenylalanine	Amino acid related
197.069		Dihydroxyphenylalanine	
197.105	C10H15NO3	methanephrine	others
202.143	C8H18N4O2	Asymmetric-dimethylarginine	Biogenic Amines
202.216	C10H26N4	spermine	alkaloids
202.216	C10H26N4	spermine	alkaloids
204.090	C11H12N2O2	Tryptophan	Amino acids
207.090	C11H13NO3	N-acetylphenylalanine	
207.126	C12H17NO2	Phenylalanine Betaine	
208.085	C10H12N2O3	Kynurenine	Biogenic Amines
211.084	C10H13NO4	methoxytyrosine	amino acids
211.084	C10H13NO4	methoxytyrosine	amino acids
213.009		3-indoxylsulfuric acid	
213.010	C8H7NO4S	3-indoxylsulfuric acid	others
214.193	C13H26O2	Tridecanoic acid	
215.116	C10H17NO4	Propenoylcarnitine C3:1	Lipids, ACYLCARNITINES
216.136	C11H20O4	Undecanedioic acid	
218.139	C10H20NO4	Propionylcarnitine C3	Lipids, ACYLCARNITINES
219.111	C9H17NO5	pantothenic acid	
220.088	C8H16N2O3S	Met-Ala	peptides
220.088	C8H16N2O3S	Met-Ala	peptides
221.090	C8H15NO6	N-acetylglucosamine	others
222.067	C7H14N2O4S	cystathionine	others
222.110	C9H18O6	Isopropyl beta-D-glucoside	
224.141	C13H20O3	Annuionone	
226.059	C9H10N2O5	Nitrotyrosine	
226.107	C9H14N4O3	Carnosine	Biogenic Amines
226.107	Carnosine		
228.111	C10H16N2O4	Hydroxyprolyl-proline	
228.209	C14H28O2	Tetradecanoic acid	
228.209	C14H28O2	Tetradecanoic acid	
228.210		Tetradecanoic acid	
229.131	C11H19NO4	Butenolycarnitine C4:1	Acylcarnitines
229.131	C11H19NO4	Butenylcarnitine	Lipids, ACYLCARNITINES
230.019	C5H11O8P	ribulose 5-phosphate	

simply_list_small_molec-7

230.152	C12H22O4	Dodecanedioic acid	Carboxylic acids
231.147	C11H21NO4	Butyrylcarnitine C4	Lipids, ACYLCARNITINES
233.126	C10H19NO5	Hydroxypropionylcarnitine C3-OH	Lipids, ACYLCARNITINES
236.137	C6H14N2O2	Lysine	Amino acids
238.084	C12H14O5	Trimethoxycinnamic acid	
238.095	C11H14N2O4	Gly-Tyr	peptides
238.095	C11H14N2O4	Gly-Tyr	peptides
240.024	C6H12N2O4S2	Cystine	Amino acid related
240.122	C10H16N4O3	Anserine	Amino acid related
242.225	C15H30O2	Pentadecanoic acid	
242.225		Pentadecanoic acid	
243.086	C9H13N3O5	cytidine	others
243.088		cytidine	
243.122	C10H17N3O4	Pro-Glu	peptides
243.147	C12H21NO4	Tiglylcarnitine C5:1	Lipids, ACYLCARNITINES
244.070	C9H12N2O6	Uridine	others
246.137	C14H18N2O2	Tryptophan betaine	
246.170	C12H24NO4	Valerylcarnitine C5	Lipids, ACYLCARNITINES
247.142	C11H21NO5	Hydroxybutyrylcarnitine C4-OH	Lipids, ACYLCARNITINES
248.119	C10H20N2O3S	Met Val	
254.225	C16H30O2	Hexadecenoic acid	
254.225	C16H30O2	FA(16:1)	fatty acids
254.225	C16H30O2	FA(16:1)	fatty acids
254.225	C16H30O2	Hexadecenoic acid	
254.225		Hexadecenoic acid	
256.240	C16H32O2	FA(16:0)	fatty acids
256.240	C16H32O2	Palmitic acid	STD
256.240	C16H32O2	FA(16:0)	fatty acids
256.241		Palmitic acid	
257.103	C8H20NO6P	glycerophosphoryl-choline	others
257.103		glycerophosphoryl-choline	
257.163	C13H23NO4	Hexenoylcarnitine C6:1	Lipids, ACYLCARNITINES
258.183	C14H26O4	Tetradecanedioic acid	Carboxylic acids
259.178	C13H25NO4	Hexanoylcarnitine C6 / Glutarylcarnitine	Lipids, ACYLCARNITINES
259.178		Hexanoylcarnitine / Glutarylcarnitine	

simply_list_small_molec-8

260.030	C6H13O9P	fructose 6-phosphate	others
260.030		fructose 6-phosphate	
260.031		fructose 6-phosphate	
260.101	C10H16N2O6	L-alpha-Glutamyl-L-hydroxyproline	
260.137	C11H20N2O5	L-gamma-Glutamyl-L-leucine, -isoleucine	
261.151		hydroxyvalerylcarnitine	
261.158	C12H23NO5	hydroxyvalerylcarnitine C5-OH	Lipids, ACYLCARNITINES
262.045	C6H15O9P	sorbitol 6-phosphate	others
262.099	C10H18N2O4S	Methionyl-hydroxyproline	
264.136	C15H20O4	Abscisic Acid	Hormones and Related
264.245	C18H32O1	9-Octadecenoic acid	
267.097	C10H13N5O4	adenosine	NT
268.081	C10H12N4O5	inosine	others
268.240	C17H32O2	Cyclohexaneundecanoic acid	
270.256	C17H34O2	Heptadecanoic acid	
273.121	C12H19NO6	Glutaconylcarnitine C5:1-DC	Lipids, ACYLCARNITINES
273.194	C14H27NO4	Heptanoylcarnitine	
275.137	C12H21NO6	Glutarylcarnitine C5-DC	Lipids, ACYLCARNITINES
276.096	C10H16N2O7	Gamma glutamylglutamic acid	
276.209	C18H28O2	Stearidonic acid	
278.225	C18H30O2	Linolenelaidic acid, punicic acid	
280.240	C18H32O2	Linoleic acid	
280.240		Linoleic acid	
280.241		Linoleic acid	
282.256	C18H34O2	Oleic acid	STD
282.256	C18H34O2	FA(18:1)	fatty acids
282.256		FA(18:1)	
282.256	C18H34O2	FA(18:1)	fatty acids
282.257		Oleic acid	
283.092	C10H13N5O5	guanosine	others
284.272	C18H36O2	FA(18:0)	fatty acids
284.272	C18H36O2	Octadecanoic acid	
284.272	C18H36O2	FA(18:0)	fatty acids
284.272		Octadecanoic acid	
285.209	C19H27NO	1-Methyl-2-nonyl-4(1H)-quinolinone	

simply_list_small_molec-9

286.230	C20H30O	pregna-5-20-dien-3beta-ol	
288.155	C10H20N6O4	Arg-Asp	
288.209	C19H28O2	Dehydroepiandrosterone	Hormones and Related
288.217	C15H30NO4	Octanoylcarnitine C8	Lipids, ACYLCARNITINES
289.153	C13H23NO6	methylglutarylcarnitine C5-M-DC	Lipids, ACYLCARNITINES
290.225	C19H30O2	Dehydrotestosterone	
290.225	C19H30O2	Nonadecenoic acid	
296.235	C18H32O3	Oxo-9-octadecenoic acid	
296.235		Oxo-9-octadecenoic acid	
296.235	C18H34O3	Oxooctadecanoic acid	
296.235	C18H34O3	Oxooctadecanoic acid	
298.251	C18H34O3	hydroxy-oleic acid	fatty acids
298.251	C18H34O3	hydroxy-oleic acid	fatty acids
299.246	C17H33NO3	Pentadecanoylglycine	
300.085	C13H16O8	Dimethyl fukiic acid	
301.056	C8H16NO9P	N-acetylglucosamine-1-phosphate	others
301.225	C16H31NO4	Nonanoylcarnitine C9	Acylcarnitines
301.225	C16H31NO4	Nonaylcarnitine	Lipids, ACYLCARNITINES
302.170	C11H22N6O4	Glu-Arg	
302.225	C20H30O2	FA(20:5)	fatty acids
302.225		FA(20:5)	
302.246	C17H34O4	MG(14:0/0:0)	
303.168	C14H25NO6	Pimelylcarnitine C7-DC	Lipids, ACYLCARNITINES
304.240	C20H32O2	Arachidonic acid	STD
304.240	C20H32O2	FA(20:4)	fatty acids
304.240		Arachidonic acid	
304.240	C20H32O2	FA(20:4)	fatty acids
304.241		Arachidonic acid	
306.155	C9H17NO4	Acetylcarnitine C2	Lipids, ACYLCARNITINES
306.183	C18H26O4	50-Carboxy-gamma-chromanol	
307.084	C10H17N3O6S	glutathione	others
308.086	C4H8N2O3	Asparagine	Amino acids
311.210	C17H29NO4	Decadienylcarnitine C10:2	Lipids, ACYLCARNITINES
312.303	C20H40O2	Arachidic acid	STD
312.303	C20H40O2	Arachidic acid	STD

simply_list_small_molec-10

313.225	C17H31NO4	Decenoylcarnitine C10:1	Lipids, ACYLCARNITINES
315.241	C17H33NO4	Decanoylcarnitine C10	Lipids, ACYLCARNITINES
316.189	C16H28O6	5(6)-Butyl-1,4-dioxan-2-one	
316.189		Linolenelaidic acid, punicic acid	
316.261	C18H36O4	(+)-15,16-Dihydroxyoctadecanoic acid	
324.036	C9H13N2O9P	Uridine monophosphate (UMP)	
324.303	C21H40O2	FA(21:1)	fatty acids
328.240	C22H32O2	FA(22:6)	fatty acids
328.240	C22H32O2	FA(22:6)	fatty acids
328.261	C19H36O4	MG(16:1	
332.272	C22H36O2	docosatetraenoic acid (22:4)	fatty acids
332.272	C22H36O2	FA(22:4)	fatty acids
338.318	C22H42O2	Erucic acid	STD
340.322	C21H42NO2	9-Hexadecenoylcholine	
341.257	C19H35NO4	Dodecenoylcarnitine C12:1	Lipids, ACYLCARNITINES
343.272	C19H37NO4	Dodecanoylcarnitine C12	Lipids, ACYLCARNITINES
346.214	C21H30O4	70-Carboxy-alpha-tocotrienol	
348.047	C10H13N4O8P	Inosinmonophosphat	Organic Acids
352.225	C20H32O5	prostaglandin E2	others
352.225	C20H32O5	prostaglandin E2	others
356.293	C21H40O4	MG(18:1/0:0)	
356.293	MG(18:1/0:0)		
360.194	C21H28O5	Cortisone	Hormones and Related
362.209	C21H30O5	Cortisol	Hormones and Related
367.272	C21H37NO4	Tetradecadienylcarnitine C14:2	Lipids, ACYLCARNITINES
368.166	C19H28O5S	Dehydroepiandrosterone sulfate	Hormones and Related
369.288	C21H39NO4	Hydroxytetradecadienylcarnitine C14:2-OH	Lipids, ACYLCARNITINES
369.288	C21H39NO4	Tetradecenoylcarnitine C14:1	Lipids, ACYLCARNITINES
370.308	C22H42O4	Diethylhexyl adipate	
370.308		Diethylhexyl adipate	
371.304	C21H41NO4	Tetradecanoylcarnitine C14	Lipids, ACYLCARNITINES
372.121	C20H20O7	Tangeritin	
373.246	C19H35NO6	Dodecanedioylcarnitine C12-DC	Lipids, ACYLCARNITINES
378.168	C20H26O7	15-Hydroxyleptocarpin, niveusin C	
378.277	C23H38O4	MG(20:4)	

simply_list_small_molec-11

378.277	C23H38O4	MG(20:4	
378.277	C25H42O4	MG(22:4	
384.339	C27H44O	desmosterol	
384.339	C27H44O	Vitamin D3, cholestenone	
385.283	C21H39NO5	Hydroxytetradecenoylcarnitine C14_1-OH	Lipids, ACYLCARNITINES
386.355	C27H46O	cholesterol	sterol lipids
386.355	C27H46O	cholesterol-H20+H	
386.355	C27H46O	cholesterol	sterol lipids
386.355		cholesterol	
386.355	C27H46O	OH-7-dehydrocholesterol	sterol lipids
388.091	C18H16N2O8	Dopaxanthin quinone	
390.277	C24H38O4	hydroxy-oxo-cholanoic acid	sterol lipids
390.277		hydroxy-oxo-cholanoic acid	
392.293	C24H40O4	Chenodeoxycholic acid	Bile acids
392.293	C24H40O4	Deoxycholic acid	Bile acids
392.293	C24H40O4	Dihydroxy-5a-cholanoic acide	
395.304	C23H41NO4	Hexadecadienylcarnitine	Lipids, ACYLCARNITINES
397.319	C23H43NO4	Hexadecenoylcarnitine	Lipids, ACYLCARNITINES
399.335	C23H45NO4	Hexadecanoylcarnitine	Lipids, ACYLCARNITINES
400.328			
400.334	C27H44O2	OH-7-dehydrocholesterol	sterol lipids
400.334	C27H44O2	cholesta-6,8(14)-dien-3beta,5alpha-diol	sterol lipids
408.288	C24H40O5	Cholic Acid	Bile acids
409.356	C25H47NO3	Octadecadienylcarnitine	Lipids, ACYLCARNITINES
410.391	C30H50	Squalene	
410.391		Squalene	
410.391	C30H50	Squalene	
411.298	C23H41NO5	Hydroxyhexadecadienylcarnitine	Lipids, ACYLCARNITINES
413.314	C23H43NO5	Hydroxyhexadecenoylcarnitine	Lipids, ACYLCARNITINES
415.330	C23H45NO5	Hydroxyhexadecanoylcarnitine	Lipids, ACYLCARNITINES
418.308	C26H42O4	110-Carboxy-alpha-chromanol	
418.308		110-Carboxy-alpha-chromanol	
418.308	C26H42O4	Hexadecyl ferulate	
420.264	C28H36O3 + Na		
420.265	C28H36O3	C28H36O3	

simply_list_small_molec-12

420.266	C28H36O3	C28H36O3 + Na	
420.266	C28H36O3	C28H36O3 + K	
420.266	C28H36O3 + K		
425.351	C25H47NO4	Octadecenoylcarnitine	Lipids, ACYLCARNITINES
427.366	C25H49NO4	Octadecanoylcarnitine	Lipids, ACYLCARNITINES
428.365	C29H48O2	Cholesteryl acetate	
428.365	C29H48O2	Cholesteryl acetate	
430.185	C21H26N4O6	Glu Trp Pro	peptides
430.185		Glu Trp Pro	
430.188		Glu Trp Pro	
431.304	C26H41NO4	Glycochenodeoxycholic acid	Bile acids
433.319	C26H43NO4	Glycolithocholic acid	Bile acids
441.345	C25H47NO5	Hydroxyoctadecenoylcarnitine	Lipids, ACYLCARNITINES
449.314	C26H43NO5	Glycodeoxycholic acid	Bile acids
449.314	C26H43NO5	Glycoursodeoxycholic acid	Bile acids
450.335	C27H46O5	Trihydroxy-5b-cholestanoic acid, coprocholic acid	
450.350	C31H46O2	Phylloquinone	
465.309	C26H43NO6	Glycocholic acid	Bile acids
465.309		Glycocholic acid	
467.301	C22H46NO7P	LysoPC(14:0)	Lipids, LYSOPHOSPHATIDYLCHOLINES,
483.302	C26H45NO5S	Taurolithocholic acid	Bile acids
493.317	C24H48NO7P	LysoPC(16:1)	Lipids, LYSOPHOSPHATIDYLCHOLINES,
495.332	C24H50NO7P	LysoPC(16:0)	Lipids, LYSOPHOSPHATIDYLCHOLINES,
499.297	C26H45NO6S	Taurodeoxycholic acid	Bile acids
499.297		Taurodeoxycholic acid	
509.348	C25H52NO7P	LysoPC(17:0)	Lipids, LYSOPHOSPHATIDYLCHOLINES,
510.465	C32H62O4	Propylene glycol mono- and diesters of	fats and fatty acids
513.276	C26H43NO7S	Glycolithocholic sulfate	Bile acids
515.292	C26H45NO7S	Tauromurocholic acid	Bile acids
515.292	C26H45NO7S	Taurocholic acid	Bile acids

simply_list_small_molec-13

515.292		Taurocholic acid	
519.332	C26H50NO7P	LysoPC(18:2)	ɔids, LYSOPHOSPHATIDYLCHOLINE
519.332		LysoPC(18:2)	
521.348	C26H52NO7P	LysoPC(18:1)	ɔids, LYSOPHOSPHATIDYLCHOLINE
523.364	C26H54NO7P	LysoPC(18:0)	ɔids, LYSOPHOSPHATIDYLCHOLINE
523.364		LysoPC(18:0)	
543.332	C28H50NO7P	LysoPC(20:4)	Lipids, LYSOPHOSPHATIDYLCHOLINES,
545.348	C28H52NO7P	LysoPC(20:3)	Lipids, LYSOPHOSPHATIDYLCHOLINES,
548.423	C37H56O3	2-Hexaprenyl-6-methoxy-1,4-benzoquinol	
564.397	C40H52O2	Carotene-3,30-dione	
570.444	C40H58O2	Dihydro-5,6-dihydroxy-carotene	
596.465	C35H64O7	Muricin C, glacin A	
607.458	C32H66NO7P	LysoPC(24:0)	Lipids, LYSOPHOSPHATIDYLCHOLINES,
610.460	C39H62O5	DG(14:1(9Z)/22:6/0:0)	
612.387	C33H56O10	Cholestane-3,7,12,25-tetrol-3-glucuronide	
617.478	C34H68NO6P	CerP(d18:1/16:0)	
620.356	C34H52O10	Pubescenin	
643.494	C36H70NO6P	Ceramide 1-phosphate	
650.600	C45H78O2	18:1 Cholesterol ester	
663.109	C21H27N7O14P2	NAD+	
664.382	C36H56O11	3-O-beta-D-Glucoside	
665.125	C21H29N7O14P2	NADH	
744.083	C21H29N7O17P3	NADP+	
750.631	C53H82O2	Plastochromanol 8	
775.645	C44H90NO7P	PC(o-18:0/18:0)	
800.653	C50H88O7	Campesterol 60-hexadecanoylglucoside	
803.677	C46H94NO7P	PC(o-18:0/20:0)	
804.721	C51H96O6	TG(14:0/18:0/16:1(9Z))	
818.736	C52H98O6	TG(16:0/15:0/18:1(11Z))	
827.677	C48H94NO7P	PC(P-18:1(9Z)/22:0)	
830.736	C53H98O6	TG(14:1(9Z)/18:0/18:1(9Z))	
831.708	C48H98NO7P	PC(o-18:0/22:0)	
838.669	C53H90O7	sterol 3-O-[6-O-(9-octadecenoyl)-b-D-glucopyranoside]	
853.692	C50H96NO7P	PC(o-22:0/22:3(10Z,13Z,16Z))	
855.708	C50H98NO7P	PC(24:1(15Z)/P-18:0)	
859.739	C50H102NO7P	PC(o-20:0/22:0)	

simply_list_small_molec-14

864.757	C57H100O5	TG(16:1(9Z)/20:5(5Z,8Z,11Z,14Z,17Z)/o-18:0)	
866.773	C57H102O5	TG(20:5(5Z,8Z,11Z,14Z,17Z)/16:0/o-18:0)	
868.788	C57H104O5	TG(18:1(9Z)/18:3(6Z,9Z,12Z)/o-18:0)	
		DAG(43:1)-H2O+H	
		Asn Asn Pro Met	peptides
		Asp Val Leu Pro	peptides
		Cys Gly Pro Val	peptides
		Met Leu Ala Thr	peptides
		Gly Glu Pro Ile	peptides
		Gly Phe Ala Tyr	peptides
		Thr Leu Gly Phe	peptides